Australian Government
Department of Defence
Defence Science and
Technology Organisation

A new Illuminator of Opportunity Bistatic Radar Research Project at DSTO

James Palmer, Simon Palumbo, Tri-Tan Van Cao and Stephen Howard

Electronic Warfare and Radar Division

Defence Science and Technology Organisation

DSTO–TR–2269

ABSTRACT

In this report a new Illuminator of Opportunity / Passive Coherent Location research project being conducted in the Microwave Radar Branch of EWRD at DSTO is discussed. Details are provided about such aspects as transmitter selection and characteristics, experimental configurations and power budget studies. Furthermore, a preliminary analysis of two different transmitters' waveform ambiguity functions is presented. Early results from field experiments demonstrating detections of cars, trucks, trains, helicopters and aircraft using a terrestrial digital TV and geosynchronous satellite signals are also presented. The ability to detect and track targets is then demonstrated through the use of several CFAR and Track Before Detect algorithms. The report concludes by discussing potential application areas for this technology as well as highlighting the likely directions of future research.

Published by

Defence Science and Technology Organisation
PO Box 1500
Edinburgh, South Australia 5111, Australia

Telephone: (08) 8259 5555
Facsimile: (08) 8259 6567

AR No. AR–014–429
May, 2009

APPROVED FOR PUBLIC RELEASE

A new Illuminator of Opportunity Bistatic Radar Research Project at DSTO

Executive Summary

In this report a new Illuminator of Opportunity / Passive Coherent Location research project being conducted in the Microwave Radar Branch of EWRD at DSTO is discussed. Details are provided about the transmitter selection and characteristics, the experimental configurations that have been, and are likely to be, used in this research and power budget studies that indicate theoretical detection ranges with the different transmitters are presented. Furthermore, a preliminary analysis of two different transmitters' waveform ambiguity functions is presented that shows the suitability of these transmitters for radar applications (i.e. their ability to estimate a target's range and Doppler).

Early results from field experiments demonstrating detections of cars, trucks, trains, helicopters and several aircraft using a terrestrial digital TV broadcast signal are also included. Furthermore, separate detections of a truck and an aircraft using a geosynchronous satellite signal are also presented. To the best of the authors' knowledge, these are the first real-world demonstrations of Passive Coherent Location detections with a geosynchronous satellite as the illuminator of opportunity.

The ability to detect targets using both terrestrial TV data and satellite data is then demonstrated through the application of Cell Averaging, Order Statistic, and Switching CFAR algorithms. The ability to track targets in terrestrial TV data is demonstrated through the application of a Histogram Probabilistic Multi-hypothesis Track Before Detect algorithm as well as a Bayesian track before detect algorithm. The report concludes by discussing potential application areas for this technology as well as highlighting the likely directions of future research.

Authors

James Palmer
EWRD

James received the Bachelor of Engineering (Electrical Hons I) and Bachelor of Arts (Japanese) degrees from the University of Queensland in 2002 and his Ph.D. in Electrical Engineering (Bistatic Radar) from the same institution in 2007. James' major research interests are in the field of bistatic radar and Inverse Synthetic Aperture Radar. James has been with the Defence Science and Technology Organisation of Australia since 2006.

Simon Palumbo
EWRD

Simon Palumbo received a Bachelor degree in Computer Systems Engineering (Hons) from Flinders University, South Australia in 2005. Since 2005, Simon has been with the Electronic Warfare and Radar Division (EWRD), DSTO, where he has been undertaking research on various radar systems, mainly focussing on software development and signal processing. From 2006 until 2008, he has undertaking a Masters degree in Defence Signal and Information Processing at the University of Adelaide and is set to complete by 2008's end.

Tri-Tan Van Cao
EWRD

Tri-Tan Van Cao graduated from Flinders University, South Australia with a Bachelor of Science (1997), a Bachelor of Biomedical Engineering (1998), and a Ph.D. in Electrical Engineering (2002) specialising in Nonlinear Automatic Control. He has been with DSTO since 2002, working mainly in the area of constant false alarm rate (CFAR) detection.

Stephen Howard
EWRD

Stephen Howard graduated in 1982 from La Trobe University, Melbourne, Australia. He received his M.S. and Ph.D. degrees in mathematics from La Trobe University in 1984 and 1990, respectively. He joined the Australian Defence Science and Technology Organisation (DSTO) in 1991, where he has been involved in research in the area electronic surveillance and radar systems. He has led the DSTO research effort into the development of algorithms in all areas of electronic surveillance, including radar pulse train deinterleaving, precision radar parameter estimation and tracking, estimation of radar intrapulse modulation, and advanced geolocation techniques. Since 2003, he has led the DSTO long-range research program in radar resource management and waveform design.

Contents

Appendices

1 Introduction

Bistatic radar has a number of advantages over monostatic radar, especially when Illuminators Of Opportunity (IOO) are employed for Passive Coherent Location (PCL). For example, IOO bistatic radar configurations do not require a dedicated transmitter, which significantly reduces implementation costs. Also, a targets' bistatic Radar Cross Section (RCS) is different [1] to its monostatic RCS, which may assist in target detection and/or classification. Furthermore, assuming suitable illuminators are available, IOO based bistatic radar allows for covert surveillance of an area of interest. In recent years a number of commercially available PCL systems have been introduced that capitalise on these advantages. Two examples are: Silent Sentry by Lockheed Martin [2] and CELLDAR by BAE Systems and Roke Manor [3].

In order to further understand the fundamental benefits and limitations of bistatic radar systems, and to understand the potential vulnerability of the Australian Defence Force (ADF) to bistatic radar, members of the Microwave Radar Branch in EWRD are constructing an IOO bistatic radar system that will initially investigate transmitters in three frequency bands: UHF, L-Band and Ku-Band; and will combine the receiver system developed for DSTO's eXperimental Phased Array Radar (XPAR) with a predominantly Commercial Off The Shelf (COTS) antenna configuration and RF front end.

Section 2 of this report presents a survey of the literature, including DSTO internal reports. This section also overviews some of the commercially available PCL systems. In Section 3, the experimental apparatus and selected illuminators are detailed. As discussed in this section, the authors' research has, to date, primarily focused on exploiting transmissions from three sources: terrestrial TV transmitters, geosynchronous satellites and, with a lesser focus at this stage, Global Navigation Satellite System (GNSS) satellites. Section 4 presents the results of power budget studies for the three selected illuminators, and gives an indication of what the maximum detection range for single-element target receivers and multi-element target receivers will likely be. In Section 5, the majority of the results of the experimental analysis and signal processing research are presented. In this section, the suitability of the waveforms of the various illuminators from a range and Doppler resolution standpoint are presented. The section then continues by presenting some real "target of opportunity" collection results. Following this, in Section 6, a brief discussion highlighting some potential application areas for PCL systems is provided. Finally, in Sections 7 and 8, the future directions of the research, and a report summary, are presented.

2 Literature Review

2.1 Papers/Texts

There are many illuminators within the urban environment, some of which are suitable for radar purposes whilst others are not. Each has its advantages for detecting targets although all of them have limitations. Ideally, the illuminator's waveforms need to produce an ambiguity function which minimises "the value of $|\chi(\tau,\phi)|^2$ (the ambiguity function) for $(\tau,\phi) \neq (0,0)$", where $|\chi(\tau,\phi)|^2$ describes "how correlated a signal is with itself delayed in time by an amount τ and shifted in Doppler an amount ϕ" [4]. This indicates that a desired response of the ambiguity function is a thumbtack response as it provides respectable estimates for both range and Doppler. Example illuminators of opportunity include terrestrial TV (both digital and analogue), satellites (Low Earth Orbit (LEO), Medium Earth Orbit (MEO) and Geosynchronous Earth Orbit (GEO)), broadcast radio (Digital Audio Broadcasting (DAB), Digital Radio Mondiale (DRM) and analogue), and mobile phone base stations.

A paper in December 1986 by Griffiths and Long [5] investigated analogue terrestrial TV as the illuminator of choice. The paper highlighted that analogue TV as an illuminator for passive bistatic radar initially would be a good choice as it has a high transmission power, a reasonably large bandwidth and a pulse like waveform. However they found in the analysis of the autocorrelation function of the TV waveform that it had high range sidelobes, and "broad peaks at 64 μs intervals corresponding to the line sync pulses" [5], thus causing ambiguities. Ringer et al. [4] concurred with these results, adding that when an echo is received from a single target, it will produce a number of returns, each separated by the 64 μs intervals. Griffiths and Baker [6] 2005 further looked at the analogue TV waveforms, adding the point that as one line of the TV picture is very similar to the next, and as there are sync pulses, range ambiguities appear at a bistatic range of 9.6 km. In 1999, a paper by Howland [7] took a different approach to using analogue TV as an illuminator of opportunity. Howland decided to use the vision or the sound carrier of the analogue TV broadcast to detect and track targets. Howland's method required no synchronisation with the TV transmitter and made use of the Doppler shift and bearing of the target echoes to estimate the target tracks. This method, seen in [7], performed a Doppler and bearing analysis which was fed into a CFAR algorithm to detect a target. The tracking was achieved by initially using a generic algorithm to get an approximate estimation of the target track, a Levenberg-Marquardt algorithm was then used to optimize the estimate and initialize the track. Finally an extended Kalman Filter was utilised to maintain the track. The results claimed that the system could detect and track aircraft targets at ranges of up to 260km, although it should be noted that later in 2005 Howland commented on this approach, stating that "the track initialization was slow and cumbersome" [8] and was limited to forward scatter applications.

Similar to the analogue TV waveform, the analogue FM radio waveforms also have a high transmit power, although they have a smaller bandwidth. Griffiths et al. [6, 9] analysed the ambiguity function of FM radio signals and concluded that the program content of the transmission determined the performance of the range and Doppler resolution. In addition they stated that the signals with high spectral content such as rock music had "the best performance, in terms of width of ambiguity function and sidelobe level" [6],

while the signals with speech modulation, in particular pauses between the words, had the worst performance. Griffiths and Baker went on to write another paper [10] which looked at the performance predictions of the FM radio signal. They predicted that with a transmit power of 250 kW, and a modulation bandwidth of 55 kHz and a 1 m^2 bistatic target RCS, a Signal-to-Noise Ratio (SNR) of 15 dB or greater could be maintained at a range of almost 30 km. In addition they predicted that when used in a multi-static environment, with another transmitter of 4 kW (e.g two transmit, one receive), the detection range was extended out to just over 30 km. Howland et al. in the same year also looked at FM radio based bistatic radar [11]. He affirmed that the greatest limitation on the system performance was the direct path Line Of Sight (LOS) interference from the leakage of its signal into the target reflected receive antenna. Thus the system's initial processing is an adaptive filter which is applied to the target reflected receive antennas to reject the direct path LOS interference. The system then cross-correlates the LOS and target reflected signals to produce a range-Doppler surface, which is fed into a CFAR algorithm to detect the target and a Kalman filter based target association algorithm [11] is used to track. The results obtained with this system demonstrated the ability to detect and track aircraft at bistatic ranges of up to 300 km.

In a different investigation, Taşdelen and Kőymen [12] examine the issues with range resolution and how to improve it. They state that "the Doppler resolution is a function of integration time, meaning that it can be improved with longer recordings. However, range resolution of this waveform cannot be improved without changing its bandwidth or waveshape." [12]. The method in which they improve the range resolution is to use multiple FM channels from co-located transmitters. Their theoretical results demonstrated that by using multiple FM broadcast channels instead of one, they were able to improve the range resolution from 6-7 km to 1 km.

As technology advanced, digital formats were introduced, allowing better ambiguity functions to be obtained. This is due to the fact that the digital transmissions are more noise-like than their analogue predecessors, and therefore more closely resemble the desired thumbtack response. Terrestrial Digital Video Broadcast (DVB-T) is one of these digital illuminators, and has been investigated by different parties as an illuminator of opportunity. Palmer et al. [13] produced a system consisting of one direct path receive antenna and one target reflective receive antenna, which detected various automotive and airborne targets at various ranges and Dopplers using the DVB-T as an illuminator of choice. Their system uses the cross-correlation technique between the direct path signal and the target reflect signal to produce range-Doppler surface plots that illustrate target detections. Zhiwen et al. [14] have written a paper on the improvement of the cross-ambiguity function using DVB-T as an illuminator of choice. As the DVB-T signal contains guard intervals and pilot peaks within the signal, these produce ambiguities in the detection process. The authors demonstrated that whilst the removal of these pulses within the signal reduced the power of the signal, (about 13.4% power loss or -0.6 dB), it improves the autocorrelation function by reducing the ambiguities.

As with the DVB-T transmissions, satellite borne illuminators utilise digital transmissions and thus are also more noise-like. In 1992 Griffiths et al. [15] proposed a system which utilised satellites as an illuminator of choice. The system consisted of a direct path and a target echo receive antenna, which were fed with modified Low Noise Block Feeds (LNBF). The LNBF's were modified so that they could have an external Local Oscillator

(LO) signal input which was synchronised to the other LO's used in the down-conversion stages, to provide coherency. The system would down-convert the receive signals to base-band I and Q form and then digitise and store the data for further processing. It would achieve processing gain by coherently cross-correlating the direct path signal and the target echo signal and then Fourier transforming, and additionally achieved incoherent processing gain by "the direct summation of the correlation output at each range bin." [15] In 2002 Griffiths et al. [16] continued with the investigation of satellite-borne illuminators. They stated that when choosing a satellite as a potential illuminator, several factors need to be considered. These were: coverage (some satellites have a fixed geographical coverage (GEO satellites) whereas some have limited temporal coverage (LEO satellites)); power density at the target ("space-based radars are significantly better than broadcast, communications or navigation systems" [16] since they transmit with more power resulting in a sufficient signal-to-noise ratio at the receiver); and finally the waveform itself. The authors designed and constructed a system which used a single antenna to receive both the direct path and the target echo signals, and separated the two in the time domain. They then used pulse compression and synthetic aperture processing to acquire detection on a target. At the time the paper was released the system had been built, integrated and tested, although no results or experiments were presented.

Another popular digital illuminator of choice are cellphone transmitters, in particular the Global System for Mobile communication (GSM) base stations. The performance of the cellphone base station transmitter was predicted in a paper written by Griffiths and Baker [10]. They predicted that when using a transmitter with an operating frequency of 1800 MHz, a modulation bandwidth of 200 kHz, a 1 square meter target RCS and a integration time of 0.1 seconds, a SNR of 15 dB can be maintained out to a range of approximately 1.2 km. Additionally they state that if the suppression of noise and the direct path interference was improved this would in turn improve the SNR and thus the maximum detectable range of a target. In 2005 Sun, Lesturgie and Chan designed and built a system using the cellphone transmitters as an illuminator of choice. The system consisted of two corner antennas, again one for receiving the direct path and one for receiving the target echoes, and an analogue and digital down conversion stage where the data was stored. In order to combat the direct path leakage and static clutter in the target reflected receiver, a least mean square based adaptive filter was utilised and then coherent cross-correlation was performed to detect targets. They found that the GSM waveform gave quite poor range resolution (approximately 1.845 km), and therefore they suggest that the GSM-based passive radar would be more suitable for Doppler detection and tracking of moving targets. It was also stated that the maximum operating range of their radar prototype was approximately several hundred metres to 1 km for ground moving targets. Kubica et al. [17] used a different approach to optimise the detection of targets using the GSM illuminator. They chose to employ a two element antenna array to passively detect the azimuth of the transmitter and then through spatial processing, attenuate the direct path interference. Therefore their processing [17] initially estimates the direction of the transmitter, and separates the direct path and target echo signals. They then attenuate the direct path signal interference in the target echo receiver and utilise clutter cancellation techniques. Two methods of target detection were investigated: an extension of a CLEAN algorithm, and an extension of an adaptive matched filter. Their results illustrated that the detection of a target was improved by both methods and they

were able to detect a high speed train with a velocity of 150 km/h.

Finally another popular illuminator of choice is the Digital Audio Broadcast (DAB) transmitter. DAB and FM modulations have similar properties to each other "although they exhibit less deterministic structures in the sidelobe regions" [9] of the autocorrelation function. Griffiths et al. [9] stated in a paper written in 2005 that although the power of the DAB signals is lower than that of FM radio, the modulation bandwidth is a lot more stable and the sidelobes exist at approximately 38 dB below the main peak. They discuss DAB further in a related paper [10], which looks at the performance predictions of DAB as an illuminator of opportunity. The prediction uses the following parameters: transmit power of 10 kW, bistatic target RCS of 1 m^2, bandwidth of 200 kHz, integration time of 100 ms, noise figure of 25 dB and losses of 5 dB. They predict that the maximum range to detect a target, with a 15 dB SNR is 9 km. They discuss further by saying that better detection ranges can be obtained by larger targets, better suppression of the exterior noise and direct path interference and improved antenna gains. Another form of digital radio transmission are the Digital Radio Mondiale (DRM) signals. Thomas et al. [18] produced an electronic letter on the analysis of the ambiguity function of the DRM signals. They state that the modulation format of the waveform is almost independent of the content that is transmitted and is "essentially a function of the modulation scheme" [18]. Thus, the ambiguity function of the waveform has thumbtack-like properties which are seen as being highly desirable. The DRM signal does have some range ambiguities due to the 400ms frame synchronisation, although these only occur at 60 000km intervals and are thus outside the detection range possible given the illuminator's power.

2.2 Commercially Available Technologies

In recent years, the technologies that support PCL have improved enormously, including greater processing power and faster analogue-to-digital (A/D) converters. This allows for more computationally advanced algorithms, greater dynamic range receiver units and, overall, a far more powerful system. As a result, several companies have introduced commercial PCL systems that capitalise on these technological advances.

2.2.1 Lockheed Martin's Silent Sentry™2

Lockheed Martin took on this passive technology and developed a multistatic surveillance radar system, which they called "Silent Sentry^{TM}2". The illuminators of opportunity that Silent Sentry 2 (SS2) utilise "to passively detect and track airborne targets in real time" [2] are FM radio transmitters, as well as analogue and digital terrestrial television transmitters. SS2 utilises a horizontal linear phased array antenna to receive the echoes from the targets, whilst also receiving on a separate antenna the direct LOS signal. Both the reference signals and the target echo signals are then utilised in signal processing algorithms to calculate the time delay between the arrival of the signals and the frequency difference of arrival (Doppler) for the signals of each target. The results from the calculations are then associated to each target and fed into a tracking filter that estimates the state vector containing the target position, velocity and acceleration. The results are then displayed or relayed to other parts of the system. The SS2 system has the capability

Table 1: *Performance of a mid-range system configuration [2]*

System Parameter	Value
Detection Range[1]	220 km
Range depth Coverage	150 km
Azimuth Coverage	60° to 360°
Elevation Coverage	50°
Target Tracking Update Rate	8 per second
Target Capacity	200+
Power Requirements	10 kW
Footprint(excluding antenna)	27 square feet

[1] Value based upon an RCS=10m^2 @ 100MHz, P_d>0.95, FAR<10^{-3}

to coarsely track a target in two dimensions when the target is illuminated by at least one transmitter, although a good two-dimensional track can be achieved when "the target is detected on two or more geometrically diverse" [2] illuminator-receive configurations. Furthermore, three-dimensional tracking of a target is possible if the target is detected on at least three geometrically diverse illuminator-receive configurations. The claimed system performance figures can be seen in Table 1. It should be noted that the performance figures displayed in this table depend on several factors, including: the geometric diversity of the illuminators, the illuminator transmission power and the RCS of the target being illuminated.

The SS2 system is available in two configurations; either as a fixed site system or as a mobile rapid deployment system. The fixed site system is a real time data processing system that is flexible in various parameters, such as the data processing rate, sampling patterns etc. The mobile system can be utilised for real time data collection as well as real time data processing. This system is not fixed in a building; but is deployed within a van that contains the target receive array on the side of the van and the LOS reference receiver antennas on the roof of the van.

2.2.2 BAE Systems and Roke Manor Research's CELLDAR

BAE Systems and Roke Manor Research have developed a passive multistatic radar system called "CELLDAR^{TM}", that uses cellphone radio waves as the illuminator of opportunity. "CELLDAR$^{\mathrm{TM}}$ uses extended multi-static radar detection and data processing for the tracking, identification and cueing of objects moving in cellphone fields" [3]. The system makes use of the radio frequencies associated with the following cellphone transmissions: GSM 900, 1800, 1900 and 3G. Although the cellphone transmissions are of low power, cellphone technology is increasing at a fast rate and their networks are rapidly gaining greater coverage, thus the ability to use cellphone transmissions to detect and track targets in a low-cost and long range radar is becoming more realisable. Cellphone tower transmitters are good illuminators as they radiate at high altitudes and in many directions. The CELLDAR system has both receive antennas (Yagi antennas) and acous-

tic detection devices, such that when the aircraft/target enters the detection region, it is detected by its echoes of the cellphone transmissions as well as by the noise it is making. A cross-correlation technique is utilised to calculate the time difference between both the LOS reference signal and the target reflected signal and thus the range and Doppler information. Roke manor has said that eventually the CELLDAR system will use phased array antennas where each of the elements will have a separate receiver and analogue-to-digital converter.

2.2.3 Thales Air Systems Passive Radars

2.2.3.1 Thales Homeland Alerter 100 (HA100)

Thales Air Systems have also exploited the advantages of passive multistatic radar systems, by developing a system that uses commercial FM radio stations as the illuminator of opportunity. Thales called this system the Homeland Alerter, or HA 100. This system, like the others, processes the signals from its illuminator of choice, FM radio, and those reflected by the aircraft/target "to compile an air picture to a range of more than" [19] a claimed 100km. The initial prototype of the HA 100 system, which was procured by the French agency DGA in 2005, had a maximum range of only 50 km, yet when Norway purchased the second HA 100 system in 2007, their radar engineers pointed out that the system was actually capable of detecting out to 100km, as there was an excessive amount of signal processing loss in the initial prototype. Thales now claims that the system is capable of "a range of more than 200 km" [20], and that it has detection performance over 360 degrees in azimuth, up to 90 degrees in elevation and ceiling up to 20000 feet [21]. They also claim that it provides three dimensional detection in position and velocity, a renewal rate of 1.5 seconds, "target classification, wake vortex detection and monitoring, and wind farm filtering" [20]. Each of the systems that have been built are installed in white Renault vans, where the receiver racks are installed in the rear of the vehicle and the signal processing hardware is installed just forward of that. The signal processing is "based on Hewlett Packard PC processors" [19], whilst a twin Ethernet link provides the ability to connect the HA 100 system "to a wider air-defence or air-traffic control network" [19]. The antenna for the Thales HA 100 system consists of eight dipoles, which are set in a circular arrangement. The antennas receive reference signals which are processed to a more accurate representation of the actual direct FM signal that was transmitted, whilst also detecting the reflected echoes off the targets and cancelling clutter and reflections from buildings.

2.2.3.2 Ground Alerter 10 (GA 10)

Thales Ground Alerter 10 or GA 10 is an omni-directional system designed to be an anti-mortar radar, thus giving warning of incoming mortar shells, and has a claimed capability of "localizing the point of impact, launch point and a rapid alarm of the threatened zone" [22]. The GA 10 consists of four UHF Yagi antennas mounted on a tripod, signal processing hardware, and a "network of autonomous sirens connected to the radar by radio connections" [23] that alert the troops to the impact zone of the mortars. Although, in comparison to the HA 100, its detection range is smaller, as it only has a claimed detection

range of 10km compared to the 200 km of the HA 100. This decrease is most likely due, in part, to the significant reduction in RCS of the mortars.

3 Experimental Program Description

3.1 Illuminators of Opportunity

The illuminators of opportunity that are under investigation in this experimental research include a terrestrial TV transmitter located at Mt Lofty in Adelaide, South Australia, the GPS satellite system, and Ku-Band geosynchronous satellites. This choice of illuminators provides a diversity in frequency, transmitter power levels and geometry, as they are spread across three frequency bands, namely UHF (TV), L-Band (GPS) and Ku-Band (geosynchronous satellites) and consist of both terrestrial, stationary satellite and dynamic satellite transmitters.

3.2 Apparatus

The equipment used for this experimental program includes a combination of COTS receiving equipment (i.e. antennas, amplifiers, etc) in conjunction with a custom DSTO-built radar receiver. The receiver belongs to the eXperimental Phase Array Radar system (XPAR) and is described in more detail below.

3.2.1 The eXperimental Phase Array Radar Receiver (XPAR)

The XPAR system digitises and extracts RF signals to a recording device for offline digital signal processing. The XPAR receiver RF chain down-converts the received signal from up to 16 independent elements to a 175 MHz nominal Intermediate Frequency (IF). Each array element has a separate 14 bit A/D converter that allows the IF signal to be digitised at 100 MS/s. The XPAR system then uses COTS chipsets to digitally down convert each IF into 32-bit complex samples. That is, it generates 16-bit in-phase and quadrature-phase samples and saves them on a large non-volatile disk. The XPAR system is capable of capturing a signal with an effective bandwidth of 10 MHz, for as long as hard disk drive space is available.

Reference frequencies used in each of the analogue and digital hardware channels are coherently locked to a single reference source. This provides the necessary coherence among the phased array elements. The XPAR analogue and digital band-pass filters provide sufficient out-of-band signal suppression such that the digitising operation is performed with minimum interference. The receiver chain for the XPAR system is illustrated in Figure 1.

3.2.2 Antenna and RF Front End Hardware

The antenna and RF front end hardware used in this program mainly consists of COTS and modified COTS components. The unmodified COTS components utilised for the DVB-T element of the system are Yagi antennas, masthead amplifiers, and channel specific band-pass filters. The geosynchronous element of the system uses offset fed satellite dishes. The LNBF's used for the geosynchronous satellites were modified such that an external local oscillator signal could be fed into their initial IF mixing stage.

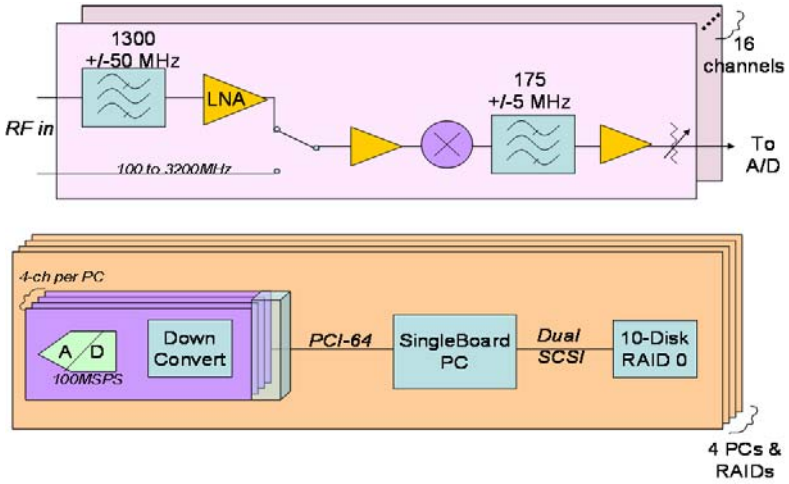

Figure 1: *XPAR Receiver Chain*

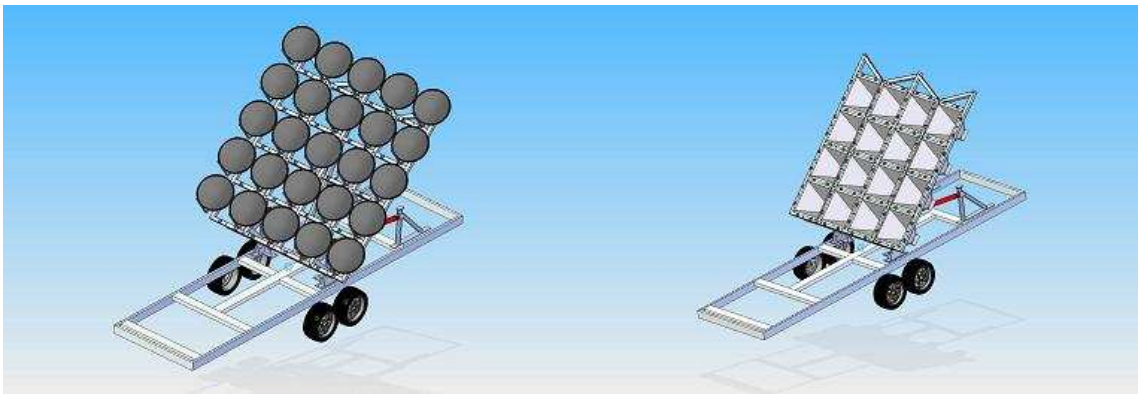

Figure 2: *Trailer Array Antenna*

3.2.3 Portable Trailer Array

As the power of both the GPS and geosynchronous satellite signals are low compared to that of the analogue and digital terrestrial television signals, other means of increasing the detection range of these signal need to be considered. One possibility is to increase the detection SNR and detection range by increasing the aperture of the antenna (i.e. through directivity gain) using an array antenna. As a result, an array antenna design was undertaken with SES. The array antenna design is based on a four by four element array. However, since the geosynchronous satellite dishes and L-Band horns are already quite large, a portable but rigid method of mounting them would be required. A trailer, the design of which can be seen in Figure 2, is believed to be the best option.

Heavily engineered, the trailer would have the capability to mount both the dishes and the horn antennas in a two-dimensional array format. The trailer could adjust the array's elevation via hydraulic arms mounted at the rear of the array face, as seen in Figure 3. Azimuthal steerability could also be incorporated. The design would also see the complete array mounted on the trailer for easy transportation to alternate sites. Whilst the trailer

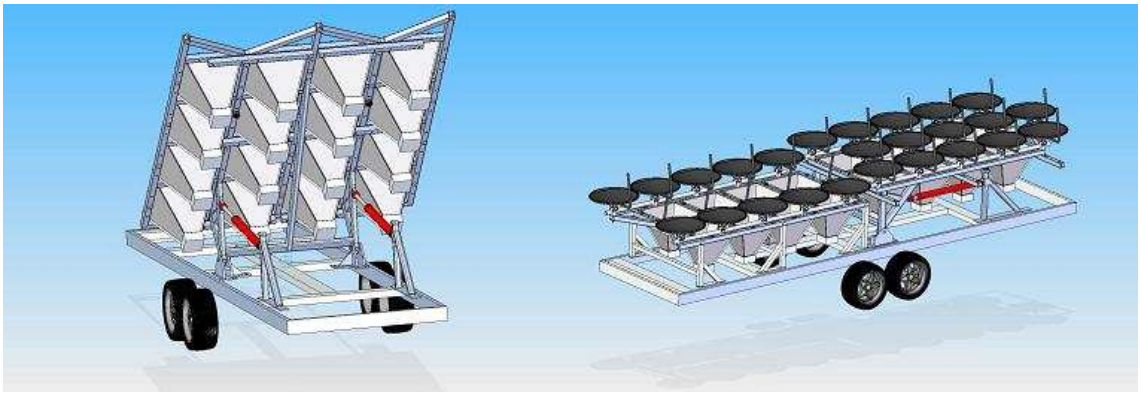

Figure 3: *Trailer Array Antenna Rear*

design is practically complete, a decision on its construction is yet to be made at the time of writing.

3.3 Experimental Configurations

A number of experimental configurations have been, and are intended to be, investigated as part of this research. These experimental configurations were initially tested in a static configuration against an active target generator, and then used in a real world target detection scenario. Truth data for the second stage of experimentation, i.e. real target detection, may be provided through a combination of outputs from DSTO's AN/FPS16 tracking radar, DSTO's Rapier tracking radar, and aircraft flight recorders. When using the high directivity gain elements, such as the Ku-Band satellite receiver dishes, ensuring that the target receiver array's time on target is sufficient may be achieved by mounting the array on a steerable mount that can be slaved to the detection coordinates provided by the AN/FPS16 radar or the Rapier tracking radar. These experiments are planned to be carried out over the next two years. Further details on the illuminator specific configurations are provided below.

3.3.1 Terrestrial TV Configuration

The configuration used for the terrestrial TV transmitter based system is shown in Figure 4, although antenna configurations ranging from 2 - 16 element linear arrays (i.e. 1 element LOS and a 1 - 15 element target reflected signal array), to 2D target reflected signal arrays (eg. 2x2, 3x3, and non square arrays) are all possible in this configuration. Note: "MHA" and "BPF" in Figure 4 stand for Mast Head Amplifier and Band-Pass Filter respectively.

3.3.2 GPS Configuration

Two configurations for the GPS based system may be investigated. The first of these configurations, shown in Figure 5, has been designed in an effort to try to improve the

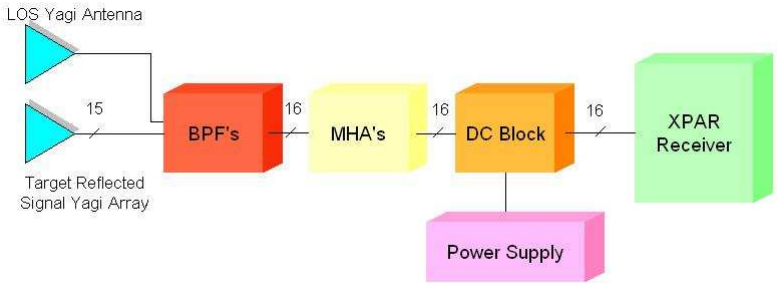

Figure 4: *Overall TV configuration*

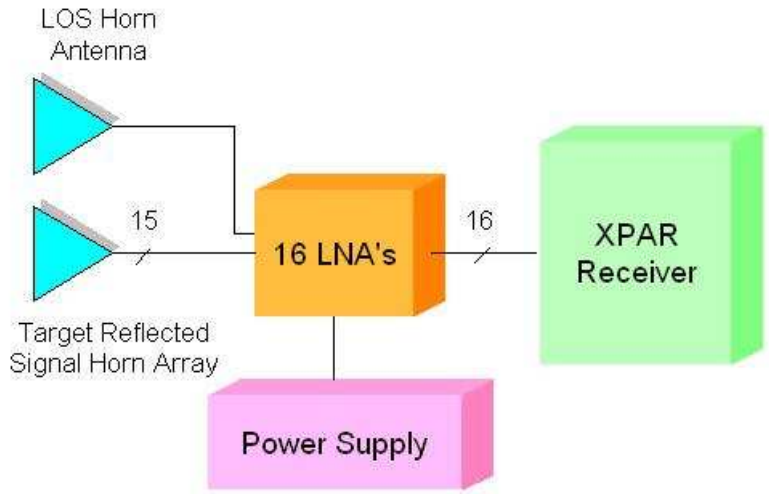

Figure 5: *Overall GPS configuration A*

detection range of the GPS based system, via the use of standard gain horns. It should be noted that in the second configuration, which is shown in Figure 6, a dedicated LOS receiver will not be used as the hemispherical pattern of the patch antennas will allow both the target and the LOS signal to be received by the array simultaneously. The second configuration has also been designed to allow the characterisation of the Left Hand Circular Polarization (LHCP) vs Right Hand Circular Polarization (RHCP) response of the target reflected signal (i.e. the quasi polarimetric response).

3.3.3 Geosynchronous Satellite Configuration

The two configurations used for the geosynchronous satellite based system are shown in Figures 7 and 8. For the experimental setup depicted in Figure 7, each antenna is a parabolic dish fed with a modified LNBF, and antenna configurations ranging from 2 - 16 element linear target reflected signal arrays (i.e. 1 element LOS, 1 - 15 element target reflected signal array) to 2D target reflected signal arrays (eg. 2x2, 3x3, and non square arrays) are likely to be investigated. For the experimental setup depicted in Figure 8, the parabolic trough reflector will be fed with a varying number of LNBF's ranging from 1 -

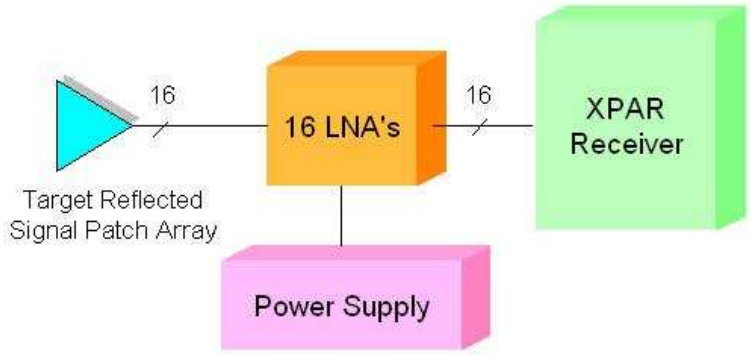

Figure 6: *Overall GPS configuration B*

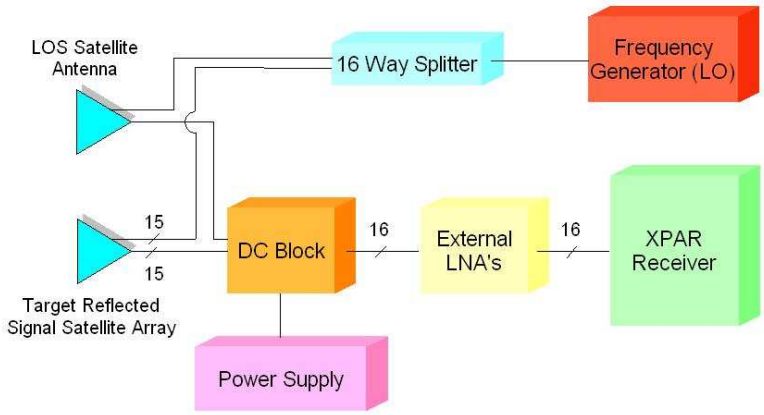

Figure 7: *Overall Geosynchronous configuration A*

15, with one other channel dedicated to the LOS signal (using a dish). The design of this trough is discussed in more detail in the following section.

3.3.3.1 Parabolic Trough Design

DSTO contracted the design and development of a 16+ element parabolic trough to the University of Adelaide via the Centre of Expertise in Phased Array and Microwave Radar systems (CEPAMiR). The following information was taken from the final report generated as part of that contract [24]. An edge-fed parabolic trough antenna 1.2 m by 2.4 m has been designed and built based on the design shown in Figure 9.

In this design, the feed-horns are placed at the focal point of the parabola. Only the top half of the parabola is used so that the feed horns can be edge mounted and therefore will not obstruct the incoming signal. The distance to the feeds (i.e. the focal point of the parabola) was designed so that the feeds are far enough away from the parabolic trough that the entire trough is within the 3 dB beamwidth of the feed horns when they are angled 20 degrees upwards. The LNBFs are spaced by 6.5 cm due to their physical size. The feeds in the array are thus spaced by 2.537λ and the array will have grating lobes at

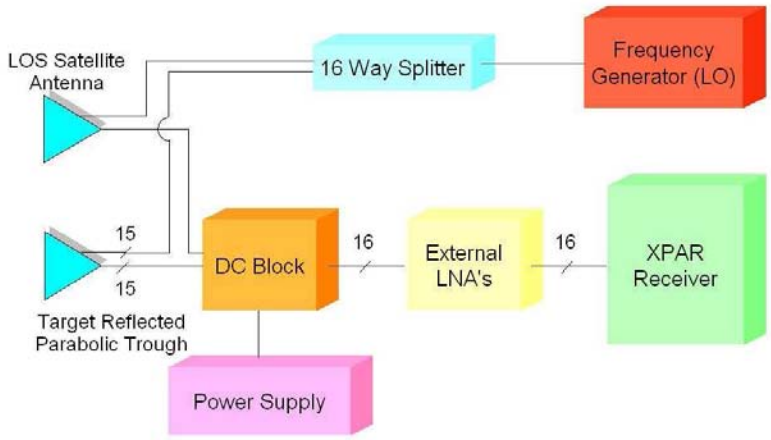

Figure 8: *Overall Geosynchronous configuration B*

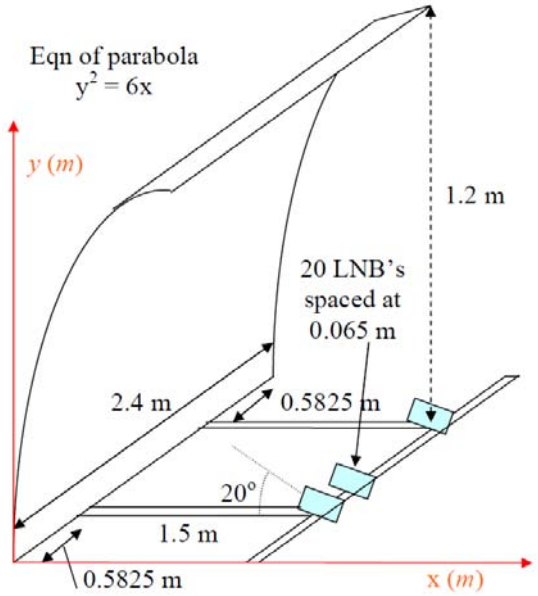

Figure 9: *Parabolic Trough Antenna (taken from [24])*

$\sin^{-1}\left(\frac{1}{2.537}\right) = 23.21°$ if the array is steered at boresight. For this steering direction the grating lobes are just outside the 20 degree beamwidth of the receiving horns, however if the beam is steered more than 1 degree either side of broadside, the grating lobes will enter the 3 dB beamwidth.

The total length of the trough is 2.4 m, and it extends approximately 58.25 cm either side of the array of feed horns. This means that the array can see angles up to $\tan^{-1}\left(\frac{0.5825}{1.5}\right) = 21.2°$ either side of the detectors, after which the reflection for the end detector moves over the edge of the reflector. This also coincides approximately with the 3 dB gain points of the feed horns.

The effective area of the entire trough antenna array is approximately 16 x 1.2 m x

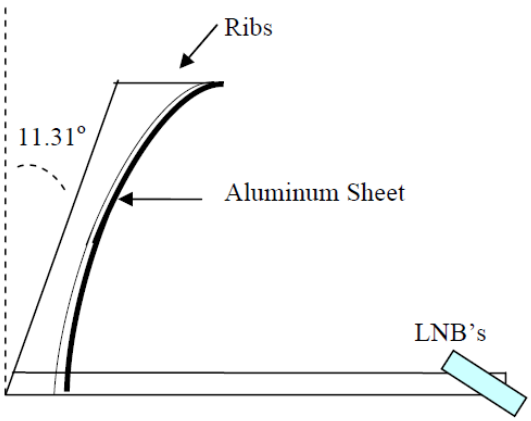

Figure 10: *Parabolic Trough Construction (taken from [24])*

0.05 m = 0.96 m^2, which corresponds to the total area of 16 strips on the reflecting surface each the width of the feed horns.

The parabolic trough was constructed from aluminium ribs which were milled to the correct shape and then covered with an aluminium sheet, as shown in Figure 10. The aluminium ribs were designed to lean forwards at an angle of 11.31 degrees to reduce the overall weight of the structure.

Pictures of the final antenna array are shown in Figures 11 and 12.

A full report on the design, construction and measured performance of the trough is given in [24].

Figure 11: *Parabolic Trough Assembly - Top down view (taken from [24])*

Figure 12: *Parabolic Trough Assembly - side on view(taken from [24])*

Table 2: *Power Budget Parameters*

Transmitter	GPS	Ku Band Geo	Terrestrial TV
Centre Frequency (GHz)	1.57542	12.5	0.5645
LOS Distance, R_{LOS} (m)	20181000	35786000	31280
SFD (dBW/m^2)	-134	-110	-48
RCS, σ (m^2)	20	20	20
τ_C (ms)	1000	100	0.4
G_R (dB)	17	38	13
L_{SP} (dB)	3.24	3.24	3.24
SNR_{MIN} (dB)	13	13	13
T_{EFF} (K)	344	344	344
Bandwidth, B (MHz)	2.046	12.5	8
G_{Array} Single	1	1	1
G_{Array} 15 element array	15	15	15
R_{MAX} (m) Single	213	990	69051
R_{MAX} (m) Array	826	3836	135892

4 Power Budget Studies

Preliminary power budget studies were carried out on the three transmitters in order to estimate what detection range performance may be expected from the systems described in Section 3. Following an approach similar to that presented in [25], the values given in Table 2 were used in conjunction with Equation 1 to determine the single antenna and 15 element antenna array maximum detection ranges listed in Table 2.

$$R_{MAX} = \sqrt{\frac{P_T.G_T.\sigma.\lambda^2.G_R.G_{SP}.G_{Array}}{(4\pi)^3.k.T_{EFF}.B.SNR_{MIN}.R_{LOS}^2.L_{SP}}} \tag{1}$$

where P_T is the transmitter power, G_T is the transmitting antenna gain, σ is the target's RCS, λ is the wavelength, G_R is the receiving antenna gain, G_{SP} is the signal processing gain (defined in equation 2), G_{Array} is the array gain, k is Boltzmann's constant, T_{EFF} is the effective system temperature in degrees Kelvin, B is the system bandwidth, SNR_{MIN} is the minimum detectable signal to noise ratio, R_{LOS} is the LOS distance between the transmitter and receiver (taken to be an estimate of the distance between transmitter and target), and L_{SP} is the loss associated with the signal processing [25].

$$G_{SP} = \frac{B}{\left(\frac{1}{\tau_C}\right)} = B\tau_C \tag{2}$$

where τ_C is the coherent integration interval.

Note: For the GPS parameters in Table 2, Signal Flux Density (SFD) values were used in the calculation of the EIRP and range values; these parameters were taken from [25, 26]. For the terrestrial TV system parameters, the Effective Isotropic Radiated Power (EIRP) value was taken from [27] and has been used to determine the signal flux density and range

values; the transmit and receive ranges were assumed equidistant. The MATLAB code used to calculate the detection ranges presented in this section may be found in Appendix A.

5 Results

5.1 Waveform Ambiguity Function Analysis

Numerous datasets were recorded in the course of the experimental field work completed as part of this research. These datasets include the LOS signals from both a terrestrial TV transmitter (including DVB-T and analogue waveforms), as well as from several geosynchronous satellites. These datasets were collected, in part, to allow the analysis of the Waveform Ambiguity Function (WAF) properties of these signals. This analysis allows us to determine the suitability of these transmitters for PCL purposes. The data was processed in MATLAB using a Doppler weighted approximation of the 2D autocorrelation process [28] (c.f. equation 3) to provide 2D WAF plots. An approximation was used for computational efficiency reasons. The Doppler weighted approach utilised a Kaiser filter for each of the illuminators. This was done for consistency over the WAF analysis and further investigation into the optimisation of the filtering will be presented in a later report. These plots are presented and discussed in the following sections. The approximation of the WAF is given by:

$$|\chi(\tau,\nu)|^2 = \left| \sum_n^N \mathbf{W}_n \int_0^{\tau_c} s\left(t' + (n-1)\tau_c\right) s^*\left(t' + (n-1)\tau_c - \tau\right) \exp\left(-j2\pi\nu t'\right) dt' \exp\left(-j2\pi (n-1)\tau_c \nu\right) \right|^2 \tag{3}$$

where τ and ν are the target delay and Doppler respectively, $\mathbf{W}_n$ are the Doppler filter weights, τ_c is the correlation segment length (coherent processing interval $T = N\tau_c$), $s(t)$ is the transmitted waveform and * denotes the complex conjugate.

5.1.1 Geosynchronous Satellite WAF Results

DVB-S data from the Optus C1 geosynchronous satellite was captured at a centre frequency of 12.59 GHz and with a bandwidth of 10 MHz (nb. this is a subset of the full bandwidth of the DVB-S signal, which, for this particular channel, is 36 MHz). 100 ms of data[1] was processed to achieve a Doppler ambiguity of 100 km/hr. This corresponds to 477 stacked 1D autocorrelations of 209 μs data segments which are then Fourier transformed. Figure 13 presents the output of this processing; i.e. a part-band DVB-S 2D waveform ambiguity function. Zero Doppler and zero range slices of this function are also provided in Figures 14 & 15. The Doppler filter weights in Equation 3, were from a Kaiser filter with a Beta of 3.5. These weights were used to achieve a consistency of approach with that of the DVB-T signal where undesirable Doppler sidelobes needed to be suppressed.

As can be seen from Figures 13 - 15, this signal provides good range and Doppler resolution and no apparent ambiguities. This suggests that this signal would be excellent for PCL purposes (due to the lack of ambiguities) but will likely result in an increased computational load due to its Doppler intolerance.

[1] Whilst this integration period was selected purely for convenience, it will be demonstrated in Sections 5.3 and 5.4 that 100 ms of coherent integration is sufficient, but not necessarily optimal, for the detection

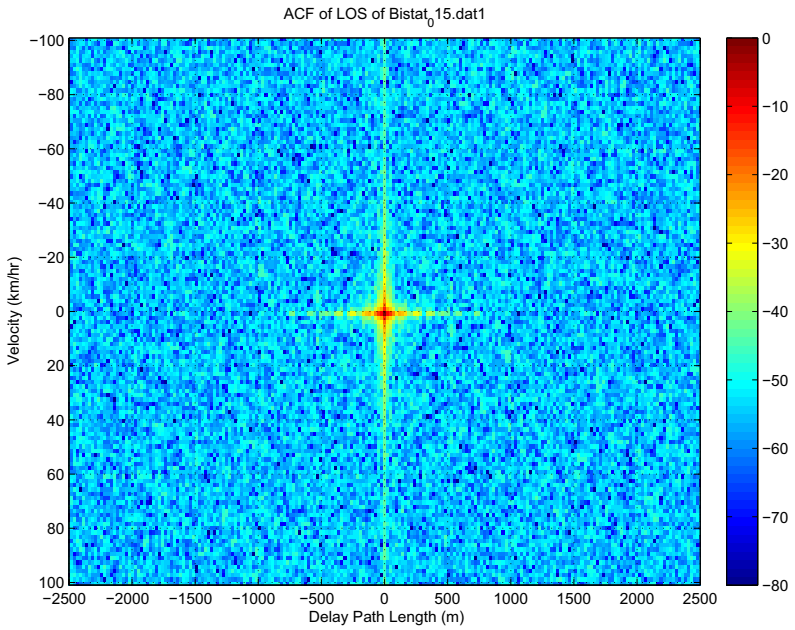

Figure 13: *2D Autocorrelation Function of the received geosynchronous satellite signal*

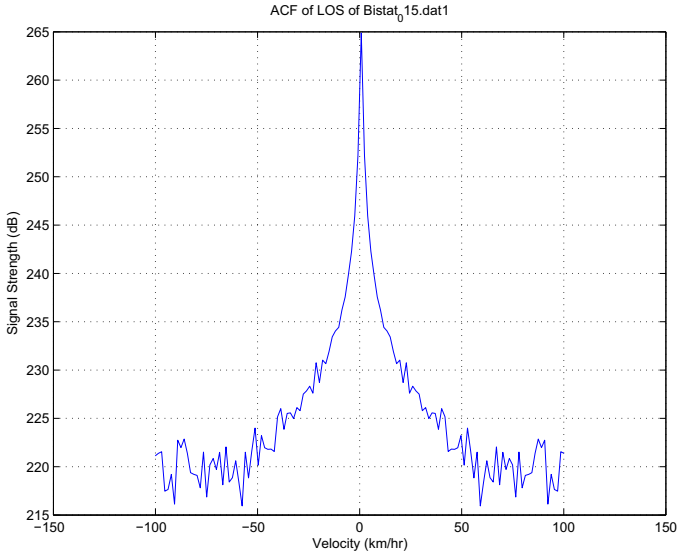

Figure 14: *Zero Path Delay (i.e. Doppler) ACF of the received geosynchronous satellite signal*

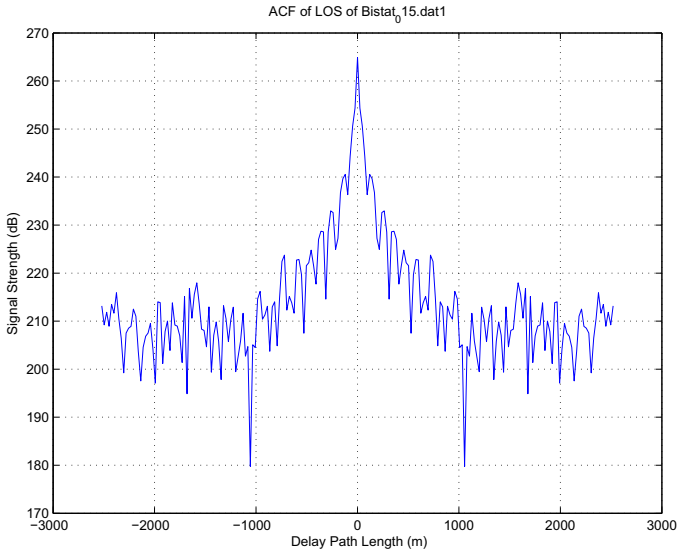

Figure 15: *Zero Doppler (i.e. Path Delay) ACF of the received geosynchronous satellite signal*

5.1.2 Terrestrial Digital TV (DVB-T) WAF Results

The TV (DVB-T) datasets have a centre frequency of 564.5 MHz and a true bandwidth of 7.5 MHz within the 10 MHz captured band. As with the DVB-S data in the previous section, this data was processed with such parameters as to achieve a Doppler ambiguity of 100km/hr. In this case, this corresponds to the stacking of 21 1D autocorrelations of 4.8ms data segments, prior to the stack being Fourier transformed. The DVB-T 2D Waveform Ambiguity Function plot is presented in Figure 16, whilst the corresponding zero Doppler and zero range slices are given in Figures 17 & 18. As with the satellite transmitter case, a Kaiser filter with a Beta of 3.5 has been applied across the Doppler dimension in order to reduce the Doppler sidelobes, and no range filtering has been applied.

As can be seen from Figures 16 - 18, this signal provides reasonable range and Doppler resolution, but may suffer from close in range ambiguities for very large RCS reflectors. Furthermore, although not present in these figures, several static range and Doppler ambiguities were noted at significantly larger ranges and Dopplers. Whilst not ideal, these ambiguities are consistent over time and are therefore manageable. These results suggest that this signal is acceptable for PCL purposes even though the ambiguities will need to be managed, and the radar signal processor will likely suffer an increased computational load due to the relatively low Doppler tolerance.

5.1.3 Terrestrial Analogue TV WAF Results

5.1.3.1 Unmodified Analogue TV Spectra Analysis

The captured terrestrial analogue TV data was originally recorded with a centre frequency

of both ground based and airborne targets with either a DVB-T or DVB-S signal

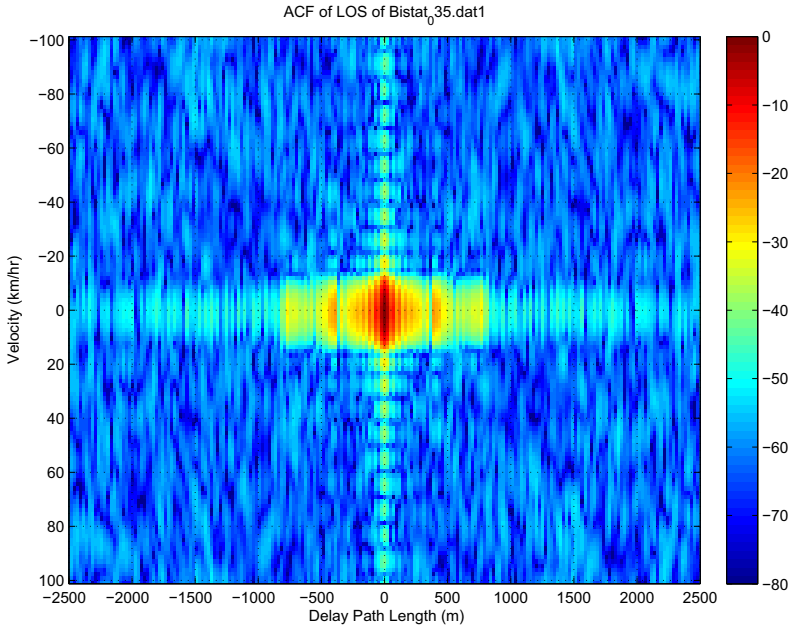

Figure 16: *2D Autocorrelation Function of terrestrial DVB-T received signal*

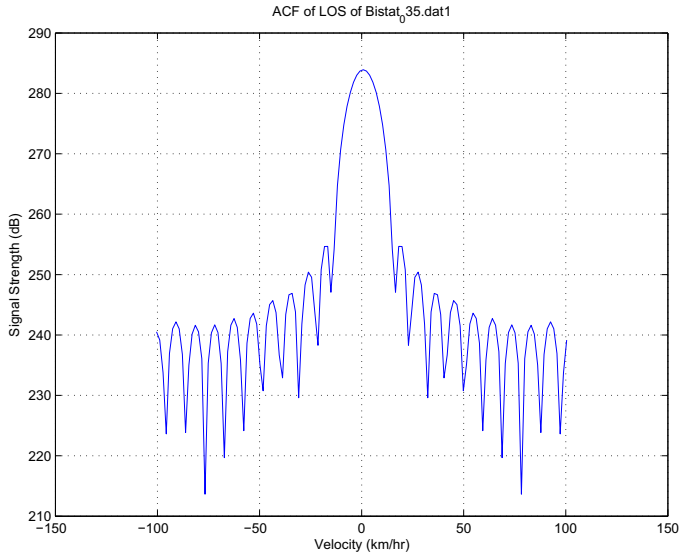

Figure 17: *Zero Path Delay (i.e. Doppler) ACF of terrestrial DVB-T received signal*

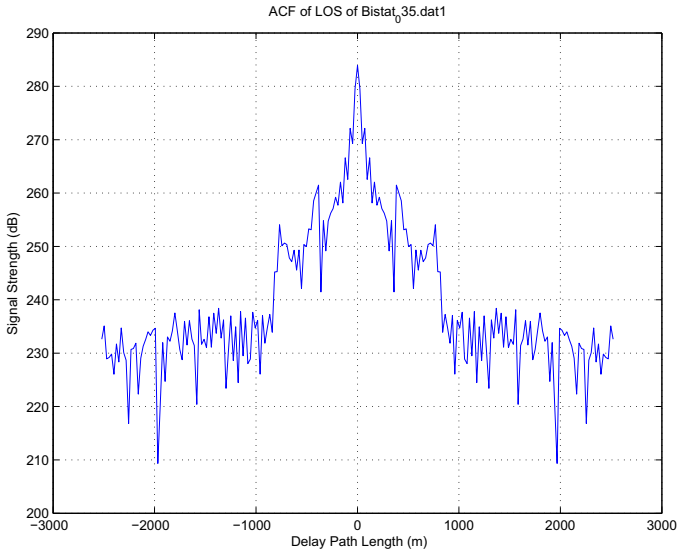

Figure 18: *Zero Doppler (i.e. Path Delay) ACF of terrestrial DVB-T received signal*

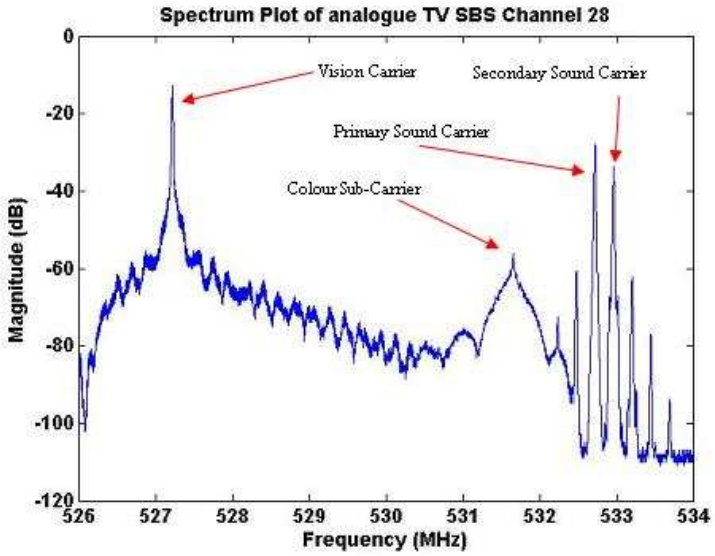

Figure 19: *Spectrum Plot of Analogue TV SBS Channel 28*

of 530 MHz with a 7 MHz bandwidth of the 10 MHz captured band. This allowed the whole channel's spectrum to be captured, containing all the carriers as seen in Figure 19.

As with the DVB-S and DVB-T data in the previous sections, this dataset was processed in order to achieve a Doppler ambiguity of 100 km/hr. The processing included stacking twenty 1D autocorrelations of 5ms data segments which were then Fourier transformed and filtered across the Doppler dimension via a Kaiser filter with a Beta of 3.5. At this stage, no range filtering has been applied. The resulting 2D WAF for the analogue TV dataset can be seen in Figure 20; the zero range and zero Doppler slices of this ambiguity function are presented in Figures 21 and 22, respectively.

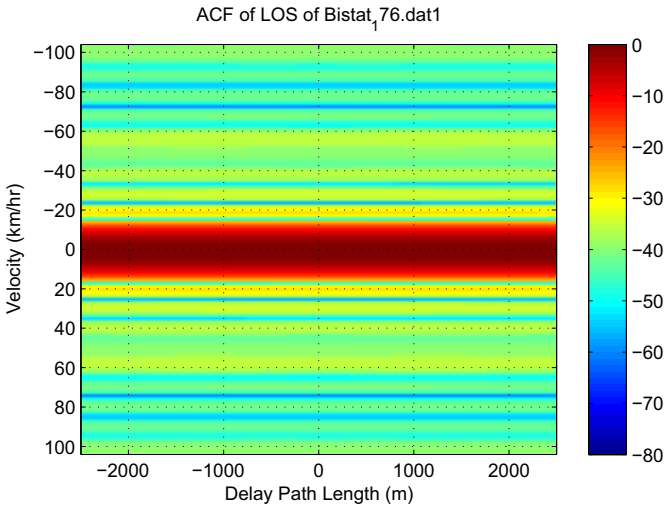

Figure 20: *2D Autocorrelation Function of the unmodified terrestrial analogue TV received signal*

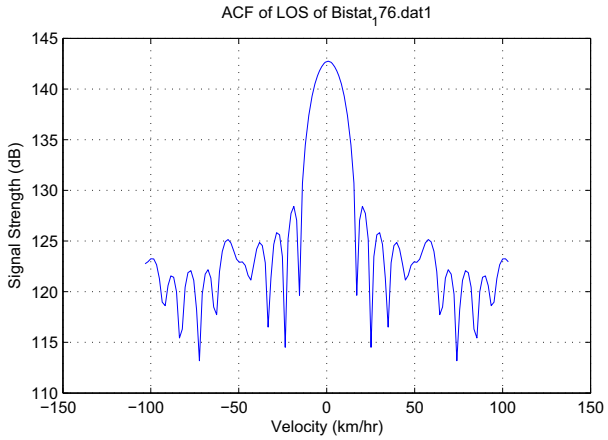

Figure 21: *Zero Path Delay (i.e. Doppler) ACF of the unmodified terrestrial analogue received signal*

From Figure 20, it can be seen that the range resolution of the 2D WAF is extremely poor. This is further shown in the zero Doppler slice, where it can be seen that the isolation of the peak from its sidelobes is not even 1 dB. The Doppler resolution on the other hand is not as inferior. The zero range slice shows that it has a wide main lobe which does reduce the Doppler resolution, although the main lobe is isolated from the sidelobes by approximately 16 dB, giving a reasonable Doppler resolution.

Various datasets were captured with centre frequencies ranging from 523 MHz up to 529 MHz, to investigate the advantages, if any, on the 2D WAF properties for different sections of the channel's spectrum. It was concluded that shifting the centre frequency did not improve the Ambiguity function results seen in Figure 20. In addition it should be noted that in these tests only part of the waveform was captured in the receivers input band, so the energy of the signal was decreased.

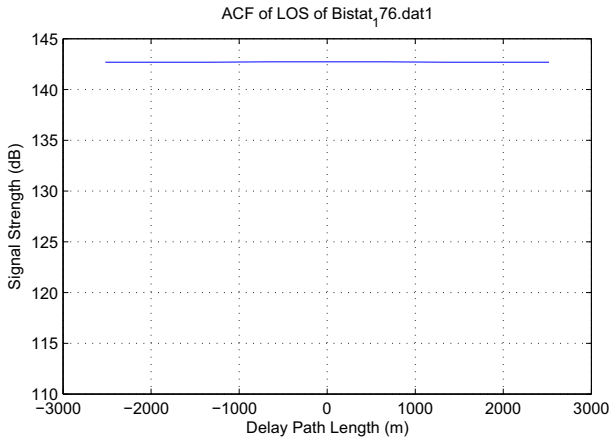

Figure 22: *Zero Doppler (i.e. Path Delay) ACF of the unmodified terrestrial analogue received signal*

5.1.3.2 Modified Analogue TV Spectra Analysis

The terrestrial analogue television unmodified spectra had a number of ambiguities when its waveform ambiguity function was analysed. Thus as some texts have said, modifying the waveform in order to improve the ambiguity function can be done with some advantages and disadvantages. The modification approach considered here was to suppress all the carriers within the spectrum that cause many of the ambiguities. When analysing the spectrum in more detail it was seen that not only were the carriers observed in Figure 19 present, there were also various signal peaks from other channels that had been mixed down in the down conversion process. The presence of these peaks is due to the fact that a band-pass filter was not used between the masthead amplifier and the antenna. Thus, there is a need for a band-pass filter in future experiments to reduce the ambiguities caused by these aliased signals. MATLAB code was written to suppress the known carriers and the aliased signals within the waveform and the resulting spectrum can be seen in Figure 23.

The peaks were suppressed in the frequency domain to the mean value of the 100 points to the left of the peak being suppressed. This allowed for the suppression of the carrier/aliased peak, whilst also allowing some of the energy within the peaks to be preserved. When modifying the waveform by suppression, the technique can cause a problem of loss of energy in the waveform, as most of the energy resides in the carrier peaks. The investigation was taken further to examine the waveform ambiguity function for each of the datasets captured with centre frequencies ranging from 523 MHz up to the 529 MHz. The datasets were analysed with the same processing techniques and parameters as explained in the unmodified analogue TV section, except for the addition of the suppression processing. It was found that when analysing the 2D WAF's and their corresponding zero range and Doppler slices, the dataset which looked to achieve the best range resolution results was the data captured at a centre frequency of 523 MHz. The resulting 2D WAF from the modified spectra, seen in the bottom half of Figure 24, indicates that the range resolution is, in fact, improved although at a cost of slightly increasing the Doppler sidelobes. It should be noted that even though it does increase the primary Doppler sidelobes

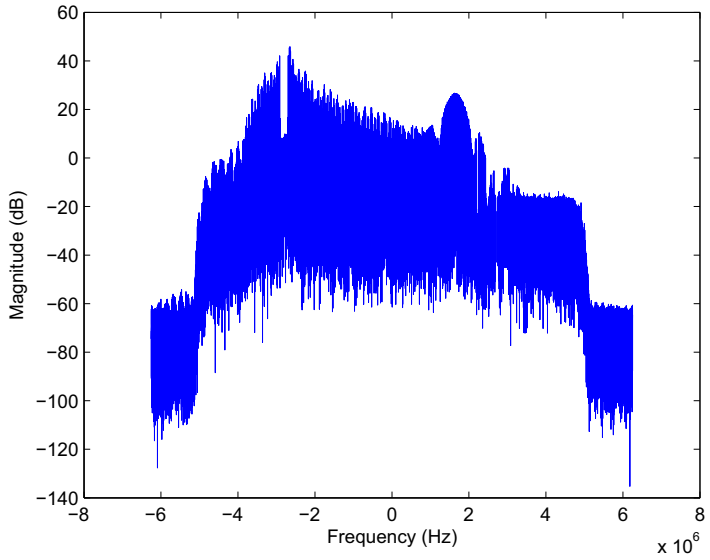

Figure 23: *Spectrum Plot of Analogue TV with suppressed carriers and aliased signal peaks*

of the main peak, the rest of the sidelobes appear to be decreased slightly, allowing a better resolution within those areas.

Further in agreement with this, the range and Doppler slices observed in Figure 25 indicate a better range resolution, although at a cost of reducing the autocorrelation peak and also increasing the sidelobes of the Doppler, thus increasing the ambiguities.

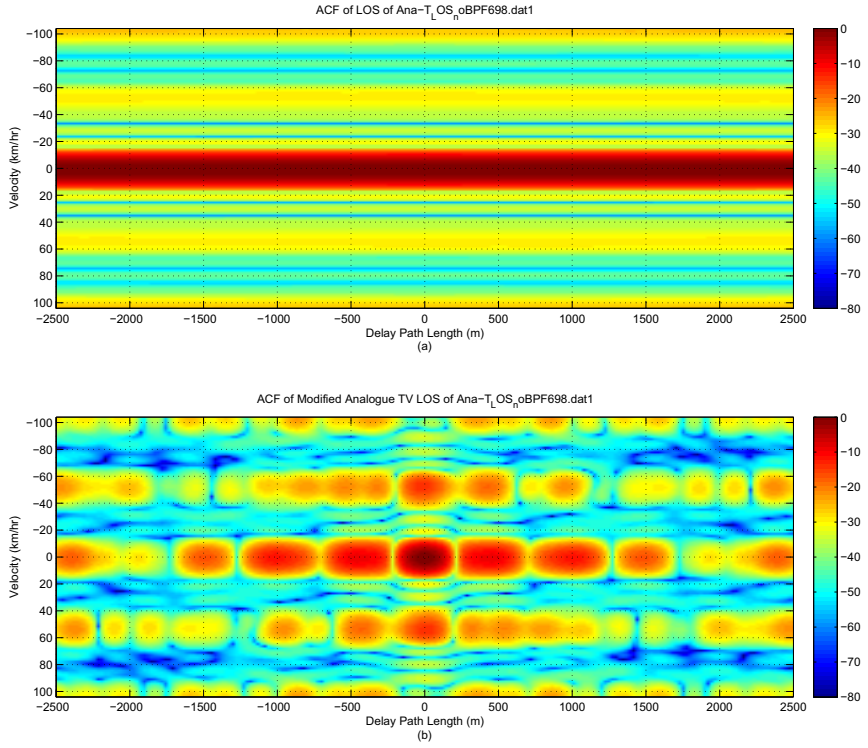

Figure 24: *2D Cross-correlation Function of the terrestrial analogue TV received signal (a) Unmodified (b) Modified*

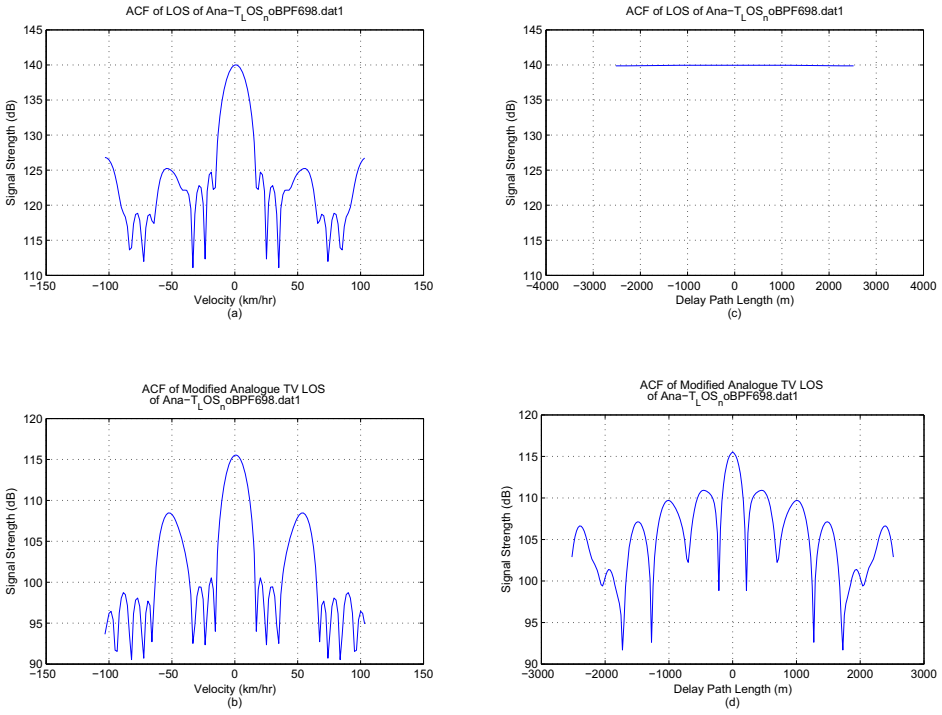

Figure 25: *Zero Path Delay (i.e. Doppler) ACF of the unmodified and modified terrestrial analogue received signal ((a), (b)) and Zero Doppler (i.e. Path Delay) ACF of the unmodified and modified terrestrial analogue received signal ((c), (d))*

5.2 Signal Processing Research

Several areas of research have been explored that may be grouped under the somewhat generic heading of "signal processing research". Some, like the empirically determined optimal coherent processing interval research, are more specific (at this stage) due to their data limited nature, whilst others, such as the outcomes of the "alias and integrate" research, are more general in their applicability.

5.2.1 "Alias and Integrate"

When exploiting the transmissions of any given illuminator of opportunity, one of the most significant fundamental limitations on the system is that of the transmitted power per Hertz. In a perfect world, the PCL system would match its receiver bandwidth to the full bandwidth of the transmitted spectrum in order to ensure that as much of the transmitted, and therefore target reflected, energy was received. Typically though, due to other limitations, such as equipment cost, the passive receiver may only be receiving a small subset of the available bandwidth. Given that the passive receiver is not generally interested in decoding the transmitted message signal, it was hypothesised that one method of receiving more of the transmitted energy was to alias the available transmitted signal into a window that matched the receiver's bandwidth. Whilst this is not considered sensible from a communications standpoint, as the message signal will be unrecoverable, this is not the intent of the typical PCL system, and is therefore an acceptable cost if it results in an increased SNR in the system's receivers. In order to test the validity of this hypothesis, several datasets were captured using a digital oscilloscope from the Optus C1 satellite using two receiver dishes simultaneously (two were used to ensure uncorrelated noise in the receiver front ends). These datasets were processed in MATLAB to mimic the effects of an aliasing operation and cross-correlated to determine the impacts on performance. As can be seen in Figures 26 - 29, the effects of aliasing the signal result in a cross-correlation strength decrease. Figures 26 and 27 show the results of a cross-correlation of an unaliased 10 MHz and 500 MHz band respectively. Whereas, Figure 28 shows the cross-correlation of two 20 MHz signals that have both been aliased into 10 MHz bands. In comparison to Figure 26, one observes a SNR reduction. Similarly, Figure 29 displays the results of a 2D cross-correlation of two 500 MHz signals that have both been aliased into a 10 MHz band. As is clearly apparent from this figure, the aliasing of this signal has resulted in a significant reduction in the SNR of the central peak.

This degradation due to aliasing has also been demonstrated theoretically, as shown below. Suppose that we have a pair of waveforms s_1 and s_2, each with bandwidth B, which are transmitted on different channels with a separation $f_d > B$. The transmitted waveform is

$$s(t) = s_1(t)e^{2\pi i f_c t} + s_2(t)e^{2\pi i (f_c+f_d)t}, \tag{4}$$

where f_c is the carrier frequency. The direct path receiver collects the signal (neglecting amplitude changes)

$$s_D(t) = s_1(t-\tau_D)e^{2\pi i f_c (t-\tau_D)} + s_2(t-\tau_D)e^{2\pi i (f_c+f_d)(t-\tau_D)}, \tag{5}$$

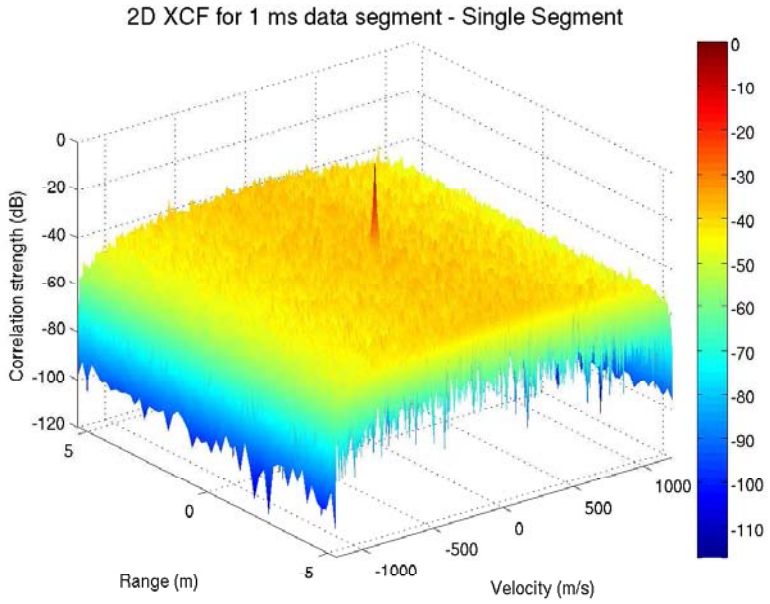

Figure 26: *Cross-correlation of two 10 MHz unaliased channels*

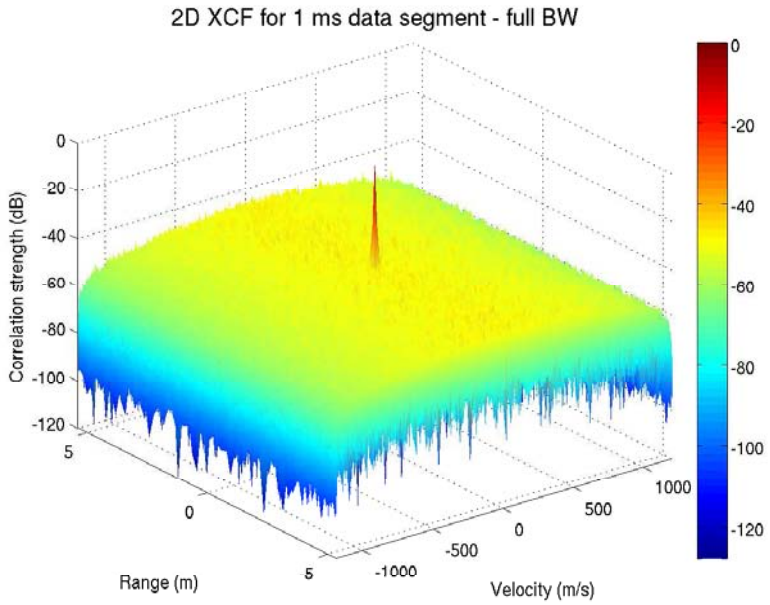

Figure 27: *Cross-correlation of two 500 MHz unaliased channels*

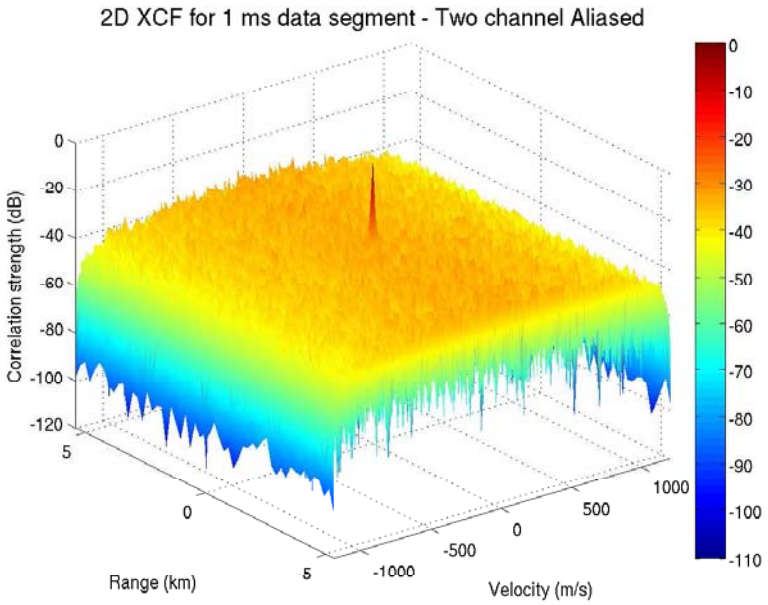

Figure 28: *Cross-correlation of two aliased channels - 20 MHz aliased into 10 MHz*

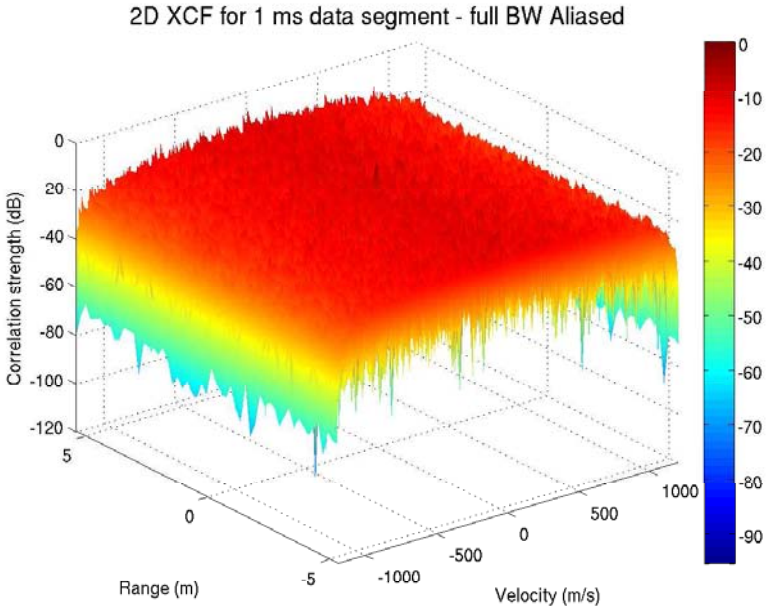

Figure 29: *Cross-correlation of two aliased channels - 500 MHz aliased into 10 MHz*

which after being down-converted and "aliased" becomes

$$\begin{aligned}\tilde{s}_D(t) &= s_1(t-\tau_D)e^{-2\pi i f_c \tau_D} + s_2(t-\tau_D)e^{-2\pi i (f_c+f_d)\tau_D} \\ &= e^{-2\pi i f_c \tau_D}\left(s_1(t-\tau_D) + s_2(t-\tau_D)e^{-2\pi i f_d \tau_D}\right).\end{aligned} \tag{6}$$

Suppose the signal is reflected by a target at an unknown position, which causes an unknown delay $\tau_D + \tau_R$, at a second antenna. The received signal at the second antenna is

$$s_R(t) = s_1(t-\tau_D-\tau_R)e^{2\pi i f_c (t-\tau_D-\tau_R)} + s_2(t-\tau_D-\tau_R)e^{2\pi i (f_c+f_d)(t-\tau_D-\tau_R)}. \tag{7}$$

which after being down-converted and "aliased" becomes

$$\begin{aligned}\tilde{s}_R(t) &= s_1(t-\tau_D-\tau_R)e^{-2\pi i f_c (\tau_D+\tau_R)} + s_2(t-\tau_D-\tau_R)e^{-2\pi i (f_c+f_d)(\tau_D+\tau_R)} \\ &= e^{-2\pi i f_c (\tau_D+\tau_R)}\left(s_1(t-\tau_D-\tau_R) + s_2(t-\tau_D-\tau_R)e^{-2\pi i f_d (\tau_D+\tau_R)}\right)\end{aligned} \tag{8}$$

Now in an attempt to detect the delay caused by the target we cross correlate the aliased signals $\tilde{s}_D$ with $\tilde{s}_R$. We obtain

$$\begin{aligned}&\left|\int_{-\infty}^{\infty} \tilde{s}_R(t)\overline{\tilde{s}_D(t-\tau)}\,dt\right|^2 \\ &= \left|\int_{-\infty}^{\infty} s_1(t-\tau_D-\tau_R)\overline{s_1(t-\tau_D-\tau)}\,dt\right. \\ &\quad + e^{-2\pi i f_d \tau_R}\int_{-\infty}^{\infty} s_2(t-\tau_D-\tau_R)\overline{s_2(t-\tau_D-\tau)}\,dt \\ &\quad + e^{2\pi i f_d \tau_D}\int_{-\infty}^{\infty} s_1(t-\tau_D-\tau_R)\overline{s_2(t-\tau_D-\tau)}\,dt \\ &\quad \left. + e^{-2\pi i f_d (\tau_D+\tau_R)}\int_{-\infty}^{\infty} s_2(t-\tau_D-\tau_R)\overline{s_1(t-\tau_D-\tau)}\,dt\right|^2.\end{aligned} \tag{9}$$

Neglecting cross correlations, which should be small if s_1 and s_2 are unrelated, we find

$$\left|\int_{-\infty}^{\infty} \tilde{s}_R(t)\overline{\tilde{s}_D(t-\tau)}\,dt\right|^2 \approx \left|R_{s_1}(\tau-\tau_R) + e^{-2\pi i f_d \tau_R} R_{s_2}(\tau-\tau_R)\right|^2, \tag{10}$$

where

$$R_{s_j}(\tau) = \int_{-\infty}^{\infty} s_j(t)\overline{s_j(t-\tau)}\,dt, \tag{11}$$

is the auto-correlation function of s_j. By contrast, cross-correlating the non-aliased signals, we find

$$\left|\int_{-\infty}^{\infty} s_R(t)\overline{s_D(t-\tau)}\,dt\right|^2 = \left|R_{s_1}(\tau-\tau_R) + e^{-2\pi i f_d (\tau-\tau_R)} R_{s_2}(\tau-\tau_R)\right|^2. \tag{12}$$

We see that at $\tau = \tau_R$, (12) has the value $|R_{s_1}(0) + R_{s_2}(0)|^2$, and the auto-correlation peaks reinforce, while the aliased cross correlation (10) has the value

$$\left|R_{s_1}(0) + e^{-2\pi i f_d \tau_R} R_{s_2}(0)\right|^2. \tag{13}$$

Here the auto-correlation peaks for s_1 and s_2 can either reinforce or cancel depending on the value of the unknown delay τ_R.

5.2.2 Forward Error Correction and the Idealised Matched Filter

Another common problem in the PCL approaches that employ the LOS signal as a reference is the presence of multipath signals and target signal leakage into the LOS reference receiver. If strong enough, the presence of these undesirable signals will introduce ambiguities in the output of the cross-correlation process and degrade the performance of the system below what theory states is achievable using the idealised Matched Filter. The hypothesis currently under test is:

> Can a system performance level significantly closer to that of the idealised matched filter be achieved by using the Forward Error Correction (FEC) codes that are present in digital (i.e. DVB-T and DVB-S) signals to remove clutter and noise from the LOS reference signal, and thereby reproduce an uncorrupted replica of the original signal (i.e. prior to transmission path degradation)?

This research is being conducted in conjunction with academics from the University of Queensland and is still in progress. Definitive results are expected within the next few months and will be presented in a follow up report.

5.2.3 RF Interference Suppression Analysis

A major issue in detecting targets in a cross-correlation process is that due to the RF interference caused by direct path and multi-path signals leaking into the target reflected channel. This causes strong peaks on the zero Doppler line at various ranges that can mask target peaks and/or cause false detections, assuming it doesn't just saturate the target receivers A/D's. In order to combat this, physical shielding techniques were employed to suppress the interference. The target reflected channel antenna was setup such that a meshed fence provided shielding from the LOS direct path signal. This produced sufficient suppression and brought the peak, caused by the interference, down to a level that was suitable for target detection and tracking. In future, when the experiments include arrays for the receive antennas, spatial cancellation of the interference signals may be employed. This would be achieved by using the array antenna to direct nulls at the interference signals; thereby giving improved suppression. Although, with this method comes a greater complexity to the system and an associated computational cost.

5.3 DVB-T Based Target Detection - Preliminary Results

Preliminary results have been processed from a single channel LOS receiver and single channel target receiver bistatic radar experimental setup. For these experiments, Adelaide's SBS Channel 33 digital terrestrial TV transmitter was used as the illuminator of opportunity. In this experiment, the only attenuation of the LOS signal afforded to the target receiver channel is that due to a small amount of shielding from a chainlink fence. As with the WAF analysis discussed in Section 5.1.1, 100ms coherent data segments were fed into a 2D cross-correlation process (see Equation 14), to produce each frame of the movies presented in Figures 30 - 36. The MATLAB code used to produce the results presented here may be found in Appendix B.

$$|\chi(\tau,\nu)|^2 = \left| \sum_n^N \omega_n \int_0^{\tau_c} s\left(t' + (n-1)\tau_c\right) r^*\left(t' + (n-1)\tau_c - \tau\right) \exp\left(-j2\pi\nu t'\right) dt' \exp\left(-j2\pi(n-1)\tau_c\nu\right) \right|^2 \tag{14}$$

where τ and ν are the target delay and Doppler respectively, ω_n are the Kaiser filter weights (across the Doppler dimension), τ_c is the correlation segment length (coherent processing interval $T = N\tau_c$), $s(t)$ and $r(t)$ are the transmitted and target reflected waveforms respectively, and * denotes the complex conjugate.

In the movies in Figures 30 and 31[2], the terrestrial TV signal was used to detect automotive traffic on a road several hundred metres from the radar setup. As can be seen in these movies, Doppler frequencies corresponding to traffic velocities of $\pm$60 km/hr were recorded. In the movie in Figure 30, 5 targets are visible; 4 with negative velocities (i.e. outbound vehicles) ranging from -30 to -60 km/hr and at ranges[3] $\sim$200 m to $\sim$1050 m and one with a positive velocity (i.e. an inbound vehicle) at roughly $\sim$250 m with a velocity of $\sim$60 km/hr. Whilst in the movie in Figure 31, we can clearly make out two large RCS targets which are due to two trucks at $\sim$300 m moving at $\sim$-50 km/hr as well as another vehicle moving in the opposite direction at $\sim$1200 m. In this movie, a range sidelobe from one of the trucks is also discernible. Given the bandwidth of this signal (i.e. 7 MHz), the maximum achievable range resolution (i.e. in the pseudo-monostatic configuration) is 20 m. In the movies in Figures 30 & 31, the bistatic angle was $\sim$45°, therefore the receiver to target range resolution was approximately 23.5 m, as determined by Equation 15:

$$\triangle r_B = \frac{c}{2B\cos\left(\frac{\beta}{2}\right)} \tag{15}$$

where $\triangle r_B$ is the bistatic range resolution for the bistatic angle, β, c is the speed of light and B is the bandwidth of the transmitted signal.

[2]Note: This document has been written for soft copy use, thus for hard copy use a single frame of the movie has been displayed

[3]All ranges presented here are path delay lengths which correspond to the path delay difference between the LOS signal and the target reflected signal; these values were not corrected to give true range from the receiver.

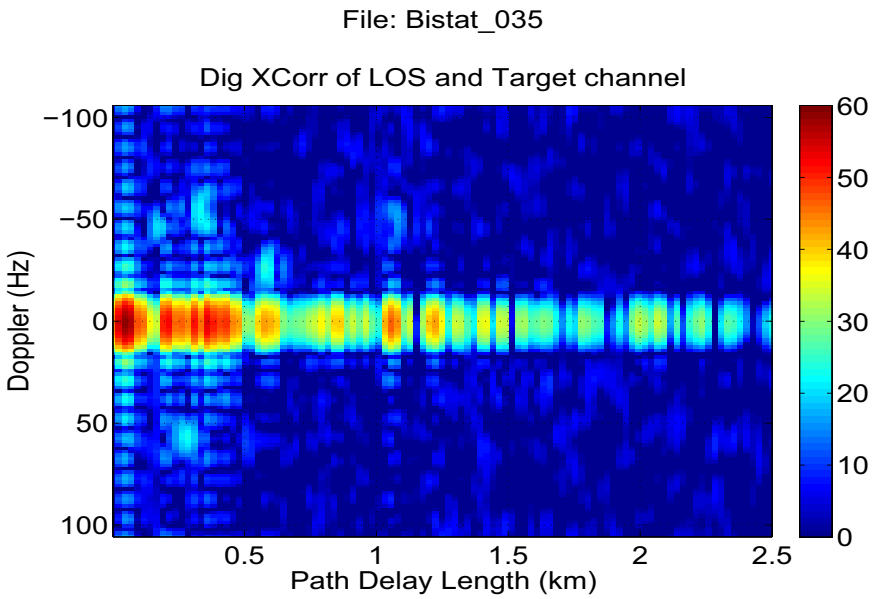

Figure 30: *Five cars - DVB-T Capture (double click the paperclip to play)*

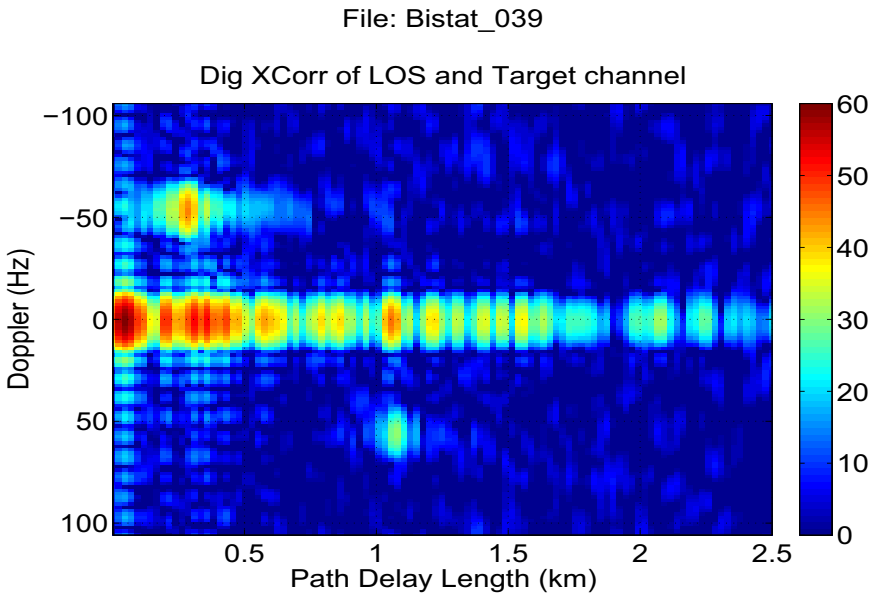

Figure 31: *Two Trucks and a car - DVB-T Capture (double click the paperclip to play)*

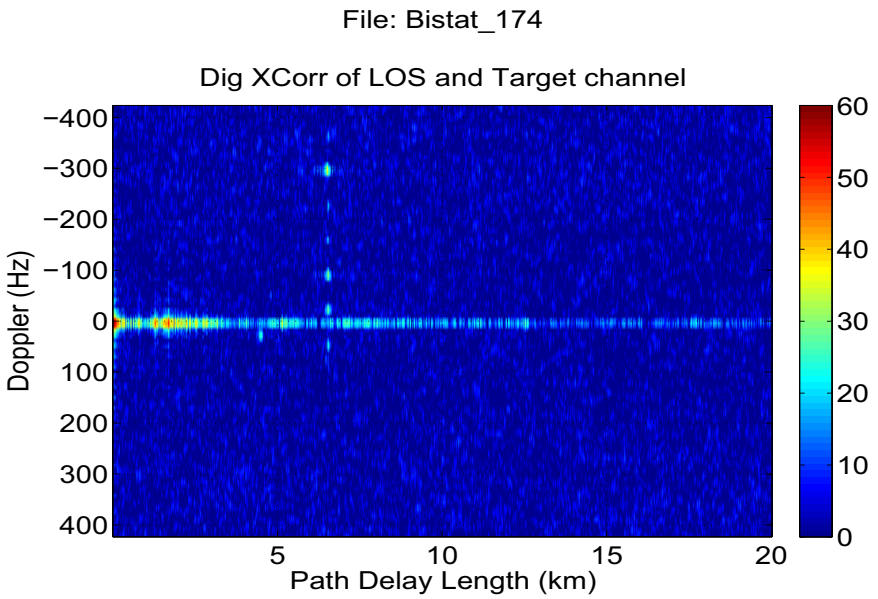

Figure 32: *Target A (see classified appendix for description) taking off - DVB-T Capture (double click the paperclip to play)*

In the movie displayed in Figure 32, an aircraft, which was taking off from a nearby airfield, is clearly discernible in both range and Doppler. As this is a propeller driven airframe, there are clearly distinguishable Doppler sidebands that are due to the modulation of the reflected signal. In the movie displayed in Figure 33, another airborne target is clearly discernible in both range and Doppler. However, as this was a jet engine driven aircraft, the Doppler sidebands are not present.

Figure 34 contains a movie showing a helicopter in flight and coming in to land. This movie clearly shows that, at times, the hub of the helicopter presents a very large RCS, and that the blade rotation results in a characteristic Doppler spread on either side of the hub. The movie in Figure 35 shows another aircraft taking off, and the movie in Figure 36 shows the same aircraft at a later point in time, and at a greater range. As is evident from these movies, each target has some relatively unique characteristics that may make classification based on this data possible. Bistatic angle estimates for the airborne targets in these movies were roughly 5 - 10°

5.3.1 DVB-T Based Target Tracking using Track Before Detect

One of the earlier datasets collected as part of this experimental campaign was processed using Track Before Detect (TBD) algorithms that were developed at DSTO. The dataset used in this work had several dynamic terrestrial targets (potentially cars, motorbikes and/or trucks), an amount of static clutter and an airborne target (of the type Target D (see classified appendix for description)). DSTO's Sam Davey and Mark Rutten applied a Histogram Probabilistic Multi-Hypothesis Tracker, (H-PMHT) [29] to the data in a proof of concept test in order to determine the suitability of PCL data for this type of track before detect process. The results are shown in Figures 37 and 38. In these figures,

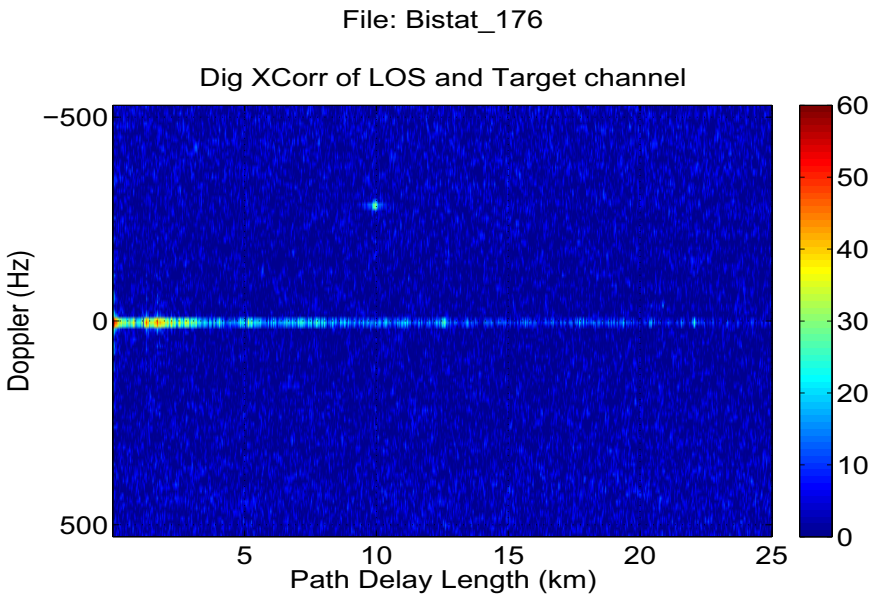

Figure 33: *Target B (see classified appendix for description) taking off - DVB-T Capture (double click the paperclip to play)*

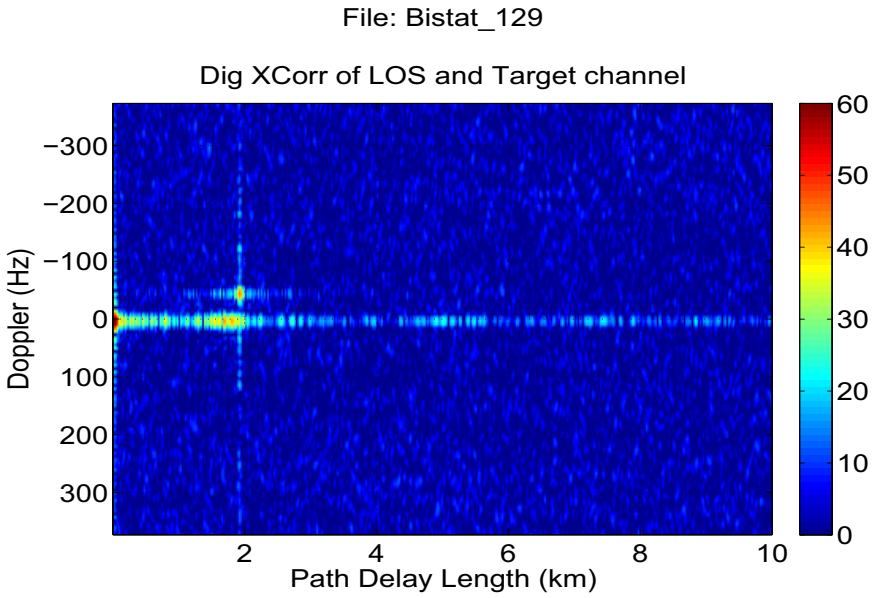

Figure 34: *Helicopter in flight and landing - DVB-T Capture (double click the paperclip to play)*

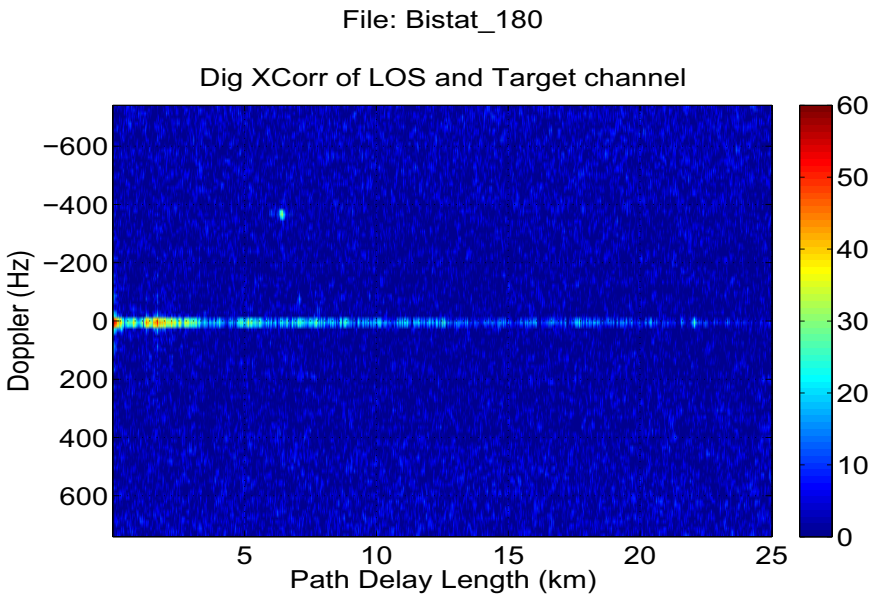

Figure 35: *Target C (see classified appendix for description) taking off - DVB-T Capture (double click the paperclip to play)*

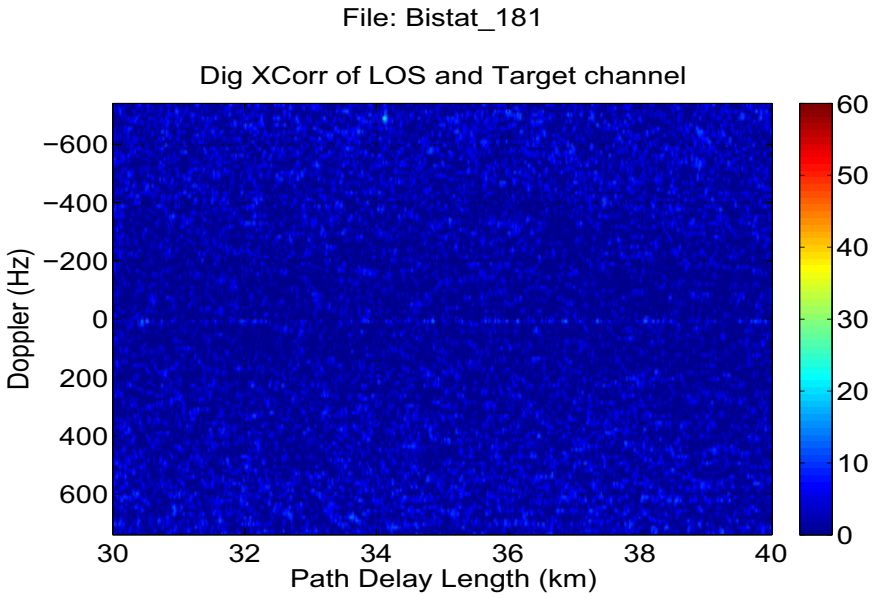

Figure 36: *Target C (see classified appendix for description) in the distance - DVB-T Capture (double click the paperclip to play)*

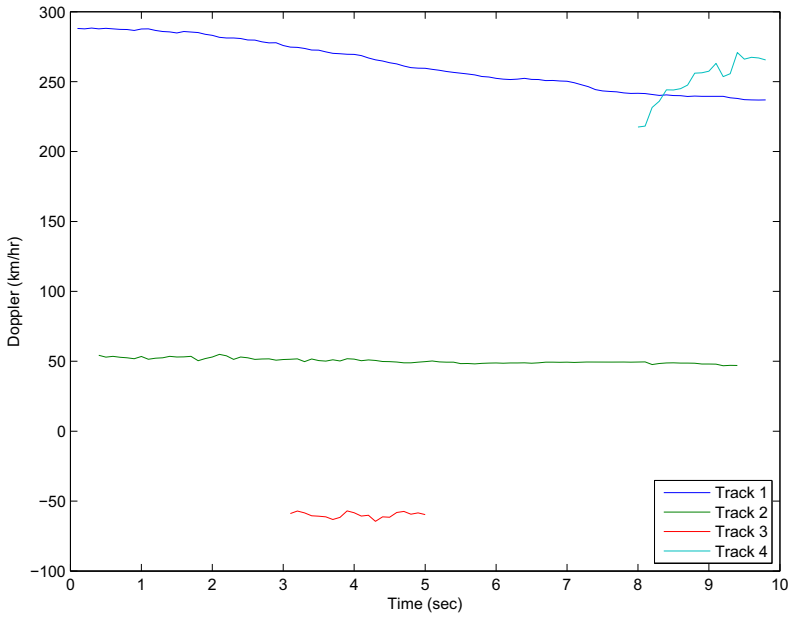

Figure 37: *Example of the tracker's Doppler history*

track 1 corresponds to a Target D type aircraft, tracks 2 and 3 are cars (travelling in opposite directions) and track 4 appears to be a false track. Movies showing the dataset used for this analysis prior to processing and with the tracks applied are given in Figures 39 and 40 respectively.

In another study, a Bayesian TBD algorithm[4], which had been developed by Paul Berry (Berry & Yau [30]) using simulated target and clutter data, was also applied to the passive radar data for the purpose of testing its performance against measured data. The algorithm was implemented in MATLAB with the aim of architectural flexibility rather than computational efficiency in order to investigate signal modelling and probability density sampling issues, and compare the detection performance of different approaches. The benefit of a TBD algorithm over conventional threshold detection is that it is able to integrate non-coherent data over multiple scans during which a target can migrate between resolution cells. This requires an implicit target motion model which embodies an assumption about how a target is likely to move. More sophisticated TBD algorithms can also estimate target velocity.

The particular signal model used works with signal amplitudes (rather than powers), assumes Rayleigh clutter statistics, Swerling 0 target and assumed known clutter power and target amplitude. A Swerling 0 target in Rayleigh clutter has a Rician distribution. The model also assumes the existence of one (and only one) target in the field of view. A Point Spread Function (PSF) characterising sensor ambiguity in range-Doppler or range-bearing is assumed given.

A window was superimposed on the range-Doppler map and the data from resolution cells contained within selected for processing. The window was chosen so as to:

[4]The authors gratefully acknowledge Paul Berry for providing this overview of Berry and Yau's work

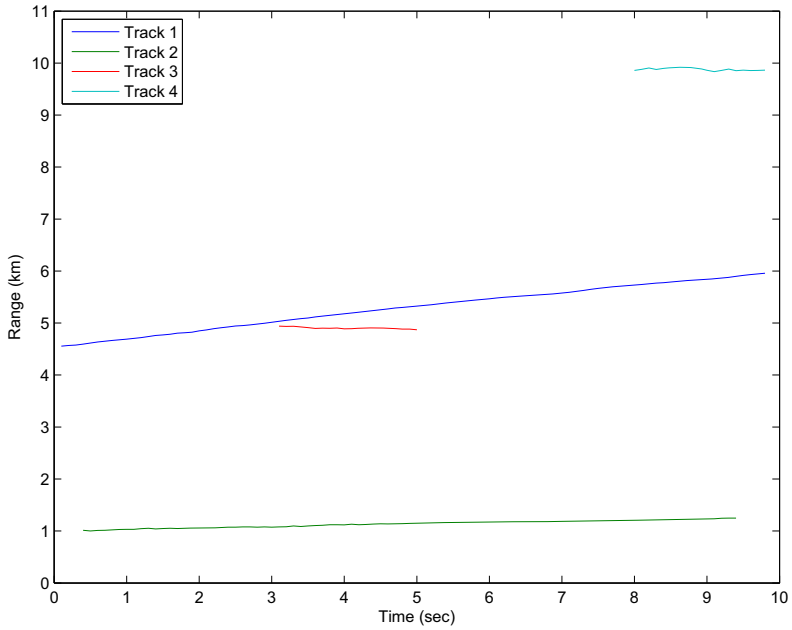

Figure 38: *Example of the tracker's range history*

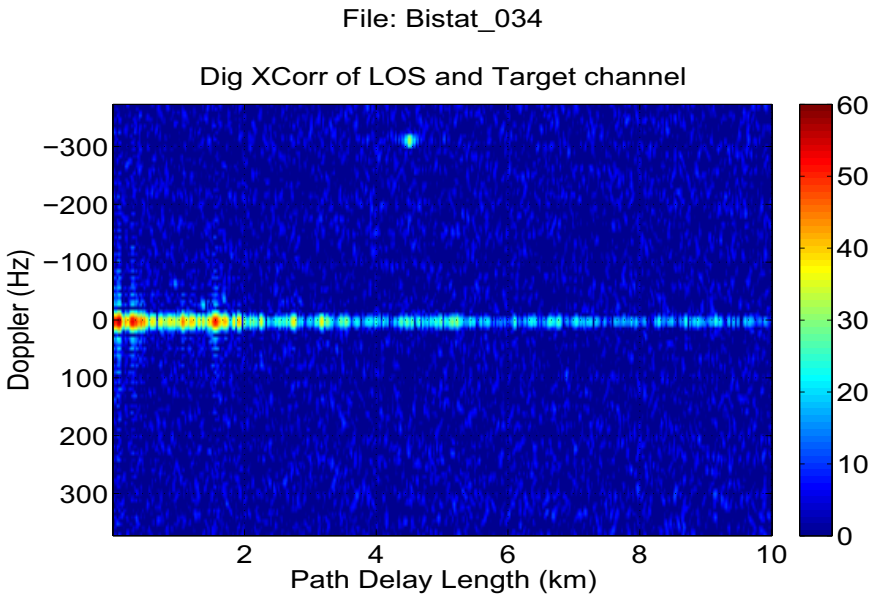

Figure 39: *Data used for tracking analysis - DVB-T Capture (double click the paperclip to play)*

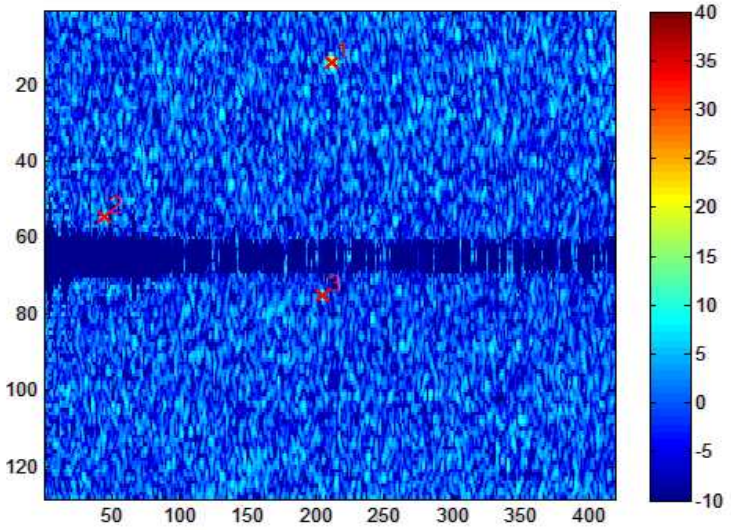

Figure 40: *Data with tracking solutions applied (double click the paperclip to play)*

1. include a single target (due to the single target assumption)

2. exclude stationary clutter

3. restrict the number of resolution cells for processing

The number of cells was restricted as the particular implementation did not employ any technique for improving the sampling efficiency such as particle filtering. The purpose of the study was to investigate the capability of Bayesian filtering but delay implementation issues until later.

Whereas the detection algorithm was optimised to the simulated scenarios in terms of target and clutter statistics and power, and sensor PSF, this was not the case when applied to the empirical DVB-T PCL datasets. Therefore this application was a test of the robustness of the algorithm. The results demonstrated that the algorithm was quickly able to 'detect' the target in the sense of estimating a Probability Density Function (PDF) with a sharp peak in the target vicinity. However, the algorithm had in its favour the fact that the Signal-to-Clutter Ratio (SCR) was quite high and the method is designed to perform in low SCR situations. Furthermore, it was found that for some data windows the algorithm broke down due to underflow. This was traced to the evaluation of the likelihood function which was numerically very small, and was due to the mismatch between the assumed and actual target and clutter power values.

Further research would focus on adaptive techniques which aim to estimate clutter power and target amplitude as well as handle multiple targets.

5.4 Geosynchronous Satellite Based Target Detection - Preliminary Results

Preliminary results from several experiments that use a single antenna LOS and single antenna target receiver bistatic radar experimental setup using the Optus C1 satellite as the illuminator of opportunity have been produced. The datasets from these experiments were processed in a manner very similar to that of the DVB-T data; the MATLAB code may be found in Appendix B. In the movies in Figures 41 and 42, the processed results of two separate data collections are displayed. In Figure 41, signals scattered from a truck driving along the road are displayed. In this experiment, a person attempted to track the truck using the target receiver's satellite dish by hand and eye. Unfortunately, as a result, it is difficult to know how long (or even if!) the target was centred in the receiver dish's mainlobe. Whilst this movie clearly demonstrates that this PCL configuration is valid, it does not begin to determine the limits of detection.

Similarly, in the movie in Figure 42, signals scattered from an aircraft preparing to land at at a nearby airfield are clearly discernible. The first notable scattered signal in this movie occurs at roughly 950 m, which, based on the power budget studies, would be approaching the maximum detection range for a 13 dBm^2 target with a 13 dB detection threshold. Whilst the bistatic RCS of this type of aircraft at Ku-band is likely to be greater than 13 dBm^2, SNR values approaching 30 dB are evident, which suggests that the maximum detection range for this target, at this bistatic angle, is likely to be much greater than the power budget suggests. Again, in this capture, it was not known if, or for how long, the target receiver dish's mainlobe was centred on the target, as this target was also being tracked by hand and eye.

The results presented in this section are, to the best of the authors' knowledge of the open literature, the first time real world targets of opportunity have been detected in range and Doppler using a satellite-borne illuminator of opportunity. Numerous authors have presented results showing the detection of skin echoes from either static ground targets or from the ocean, whilst other authors have presented (theoretical) calculations of power budget studies for aircraft detection. Only two authors have presented anything that may be considered similar to the results presented here. In [31], Koch and Westphal demonstrated the detection of airborne targets using GPS signals. However these detections were along the forward scatter path and therefore provided no estimate of the target's range or velocity. Similarly, Cherniakov et al [32] have presented results indicating the detection of a static helicopter on the ground with rotating blades but in a very contrived experiment and at much shorter ranges. Their approach also required incoherent integration intervals between 4 and 22 s to achieve a detection. These incoherent integration intervals are likely to be too long for the real world detection of dynamic targets as has been demonstrated here. Note, no incoherent integration was used in the processing presented here.

5.5 Application of Constant False Alarm Rate (CFAR) Detectors to PCL data

A common routine test in any detection system is to compare the received signal level with a pre-defined threshold value. In modern radar detection, the decision on target

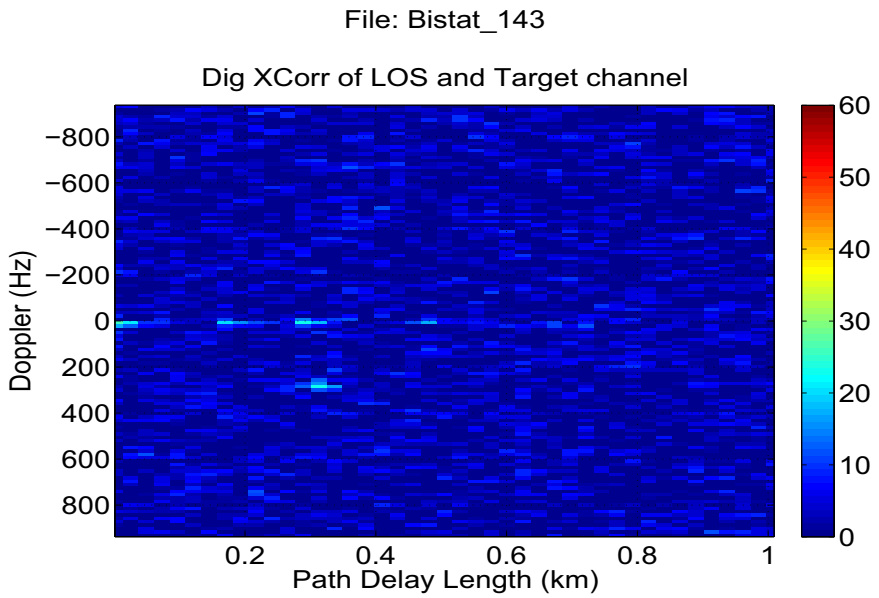

Figure 41: *Truck driving along the road - DVB-S Capture (double click the paperclip to play)*

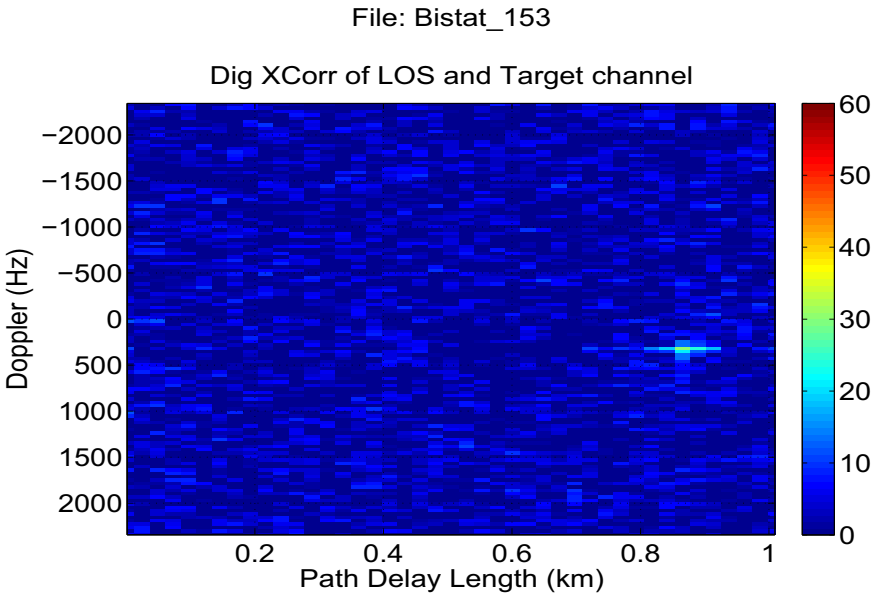

Figure 42: *Target A landing (see classified appendix for description) - DVB-S Capture (double click the paperclip to play)*

presence or absence is often performed automatically, i.e., without the visual intervention of the radar operator. When the threshold is a fixed value, the false alarm rate will increase intolerably (i.e., beyond a level the computer inside an automatic detector can handle) as the interference power varies. Therefore, a Constant False Alarm Rate (CFAR) algorithm with an adaptive threshold is required to keep the false alarm rate to a manageable level [33]. In this section, applications of different CFAR detectors to a representative set of bistatic PCL radar data is performed.

5.5.1 CFAR Introduction

The most basic form of a CFAR processor is the *Cell-Averaging* CFAR (CA-CFAR) [34]. Input to the processor is the envelope (or square-law) detected output which is sampled in range (and Doppler if possible). Each sample in the range/Doppler dimensions is called a *cell*. Figure 43 shows an implementation of the CA-CFAR detector. The signal magnitude x_0 in the test cell (where a decision on target presence or absence has to be made) is compared to a threshold formed by multiplying the interference estimate with a constant α, the value of which is determined by the required false alarm rate. The interference is estimated using the surrounding cells $x_1, x_2, \ldots, x_{2N}$ (which are termed reference cells) and is simply the summation of those $2N$ reference samples. A few immediate neighbours (known as guard cells) on each side of the test cell are excluded from the estimation to prevent possible power spillover from the test cell.

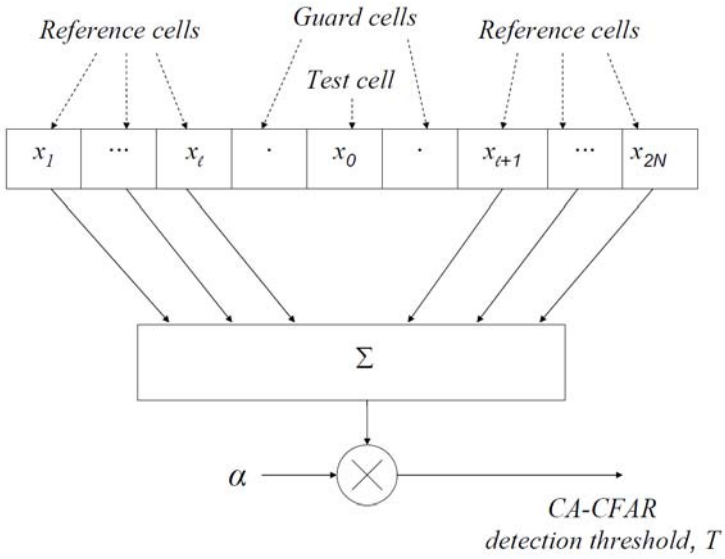

Figure 43: *Cell-Averaging Constant False Alarm Rate (CA-CFAR) detection*

Under the condition that the reference samples are independent and identically distributed (iid) and are governed by the exponential distribution, the performance of the CA-CFAR processor is optimal in the sense that the detection probability is maximised for a given false alarm rate [34]. In practice, there are two common situations when the IID assumption no longer holds: (i) there is a clutter edge (e.g., at the border of land and sea),

where the energy of interference changes, and (ii) there is an outlier, e.g., a clutter spike, an impulsive interference, or another interfering target. These can result in the masking of weaker targets near stronger targets, excessive false alarms at clutter transitions, and missing of targets near clutter edges.

There are a variety of robust substitutions to CA-CFAR [35], for instance, the smaller-of CFAR, which is designed to improve target detection in the presence of multiple targets by splitting the reference window into a leading part and a lagging part and then selecting the part with a smaller sample sum for threshold computation; the greater-of CFAR which is designed to minimise the false alarm rate at a clutter edge (by selecting the part with a greater sample sum); the Order Statistic CFAR (OS-CFAR), where the interference estimate is given by the amplitude of the k^{th} ordered reference sample; the Switching CFAR (S-CFAR) where the sample in the test cell is used to select appropriate reference data [36], etc. Each of these modified CFAR algorithms, however, has its own advantages and drawbacks, depending on the operating environment and the statistical model of both target and clutter returns. They all, nevertheless, have the same design methodology in that a censoring operation is made to eliminate inappropriate reference samples in a nonhomogeneous environment.

In the following sections, the applications of CA-CFAR, OS-CFAR, and S-CFAR are discussed. Based on Rayleigh clutter and Swerling I target models, parameters of the CA-CFAR and OS-CFAR are computed using the closed-form formula presented in [35], while those of the S-CFAR are derived as in [36]. For all three CFAR detectors, the false alarm is set at 10^{-6}. Two guard cells on each side of the test cell are used to avoid signal spillover from the test cell. $2N = 16$ reference cells (8 on each side of the test cell) are used in the computation of adaptive thresholds, so that a detection probability of approximately 70% is achieved for a target of SNR 20 dB.

5.5.2 Design of CFAR Detectors

5.5.2.1 CA-CFAR Design

Given the set of $2N$ reference samples $\mathbf{X} = \{x_1, x_2, \ldots, x_{2N}\}$ (see Figure 43), the CA-CFAR detection threshold is:

$$T_{CA} = \alpha \times \sum_{n=1}^{2N} x_n \tag{16}$$

For $2N = 16$, the threshold multiplier is set to $\alpha = 1.3725$ in order to give a false alarm of $P_{fa} = 10^{-6}$ as required.

5.5.2.2 OS-CFAR Design

The detection threshold for an OS-CFAR detector is formed as:

$$T_{OS} = \alpha \times x_{(k)} \tag{17}$$

where $x_{(1)} \leq x_{(2)} \leq \cdots \leq x_{(k)} \leq \cdots \leq x_{(2N)}$ are the ordered reference samples. In this application, parameters of the OS-CFAR are set to $\alpha = 20.95$, $k = 12$ to give a false alarm

$P_{fa} = 10^{-6}$ and so that the detector can tolerate up to 4 interfering samples in the set of reference samples.

5.5.2.3 S-CFAR Design

The detection procedure for an S-CFAR detector is as follows. Firstly, $2N$ reference samples are partitioned into two sets S_0 and S_1:

$$x_n \underset{S_0}{\overset{S_1}{\gtrless}} \alpha x_0, \tag{18}$$

i.e., a reference sample x_n, $n = 1, 2, \ldots 2N$, either belongs to the set S_0 if it is less than the value αx_0, or belongs to the set S_1, otherwise. Secondly, let n_0 be the number of samples contained in S_0, a target is declared in the test cell if:

- (i)
$$x_0 > \frac{\beta}{n_0} \sum_{x_n \in S_0} x_n, \quad when \quad n_0 > N_T, \quad \textbf{or} \tag{19}$$
- (ii)
$$x_0 > \frac{\beta}{2N} \sum_{k=1}^{2N} x_n, \quad when \quad n_0 \leq N_T \tag{20}$$

where x_0 is the amplitude of the sample in the test cell; α, β, and N_T are three constants the values of which are set based on the required false alarm rate. In this application, these three parameters are set as $\alpha = 0.4$, $\beta = 24.55$, and $N_T = 11$ to give a false alarm $P_{fa} = 10^{-6}$ and so that the detector can tolerate up to 4 interfering samples in the set of reference samples. A detailed procedure for selecting those parameters is described in [36].

5.5.3 Application of CFAR Detection to the Experimental Data

5.5.3.1 DVB-S Detection of Target A

The data file analysed here consists of 199 frames. Each frame is a 64×128 complex number matrix representing a range-Doppler map. A target first appears in frame 96 at range 1010 m, Doppler 1500 Hz as indicated by the arrow in Figure 44. The CFAR detection of this target from frame 96 to frame 199 is shown in Figure 45. For each Doppler index, the thresholding tests are only performed at path delay lengths from 250 m to 1250 m where a CA-CFAR sliding window detection with $2N = 16$ can be fitted in. CA-CFAR and S-CFAR detectors give the same performance as shown in Figure 45(a), and are therefore not shown here. It is clear that the target has a trajectory extended from range 1010 m to range 840 m, with a decrease in Doppler frequency from 1500 Hz to 0 Hz (i.e., zero radial velocity). A false alarm at range=480 m, Doppler=0 Hz is also evident.

This false alarm can be resolved based on its zero Doppler which most likely indicates a clutter spike in the mainlobe clutter. Performance of the OS-CFAR is shown in Figure 45(b). Although OS-CFAR does not give the false alarm at Doppler zero, it misses nearly the whole trajectory of the target.

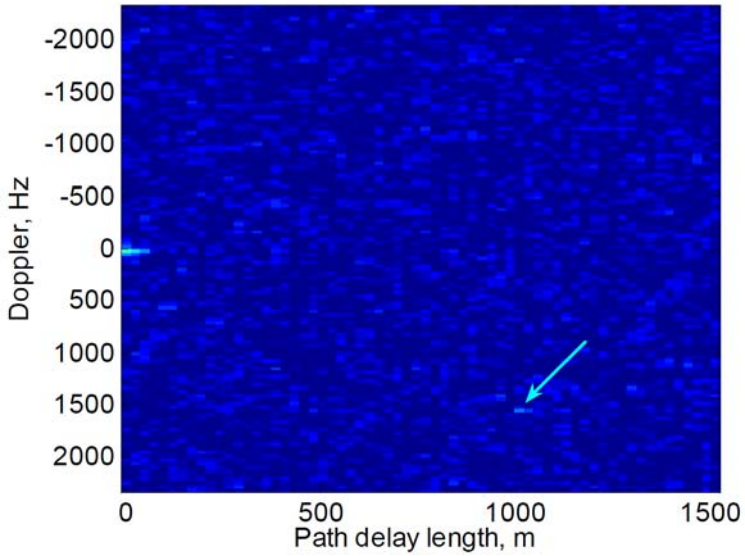

Figure 44: *Frame 96 of a DVB-S data file with a target at range=1010 m, Doppler=1500 Hz*

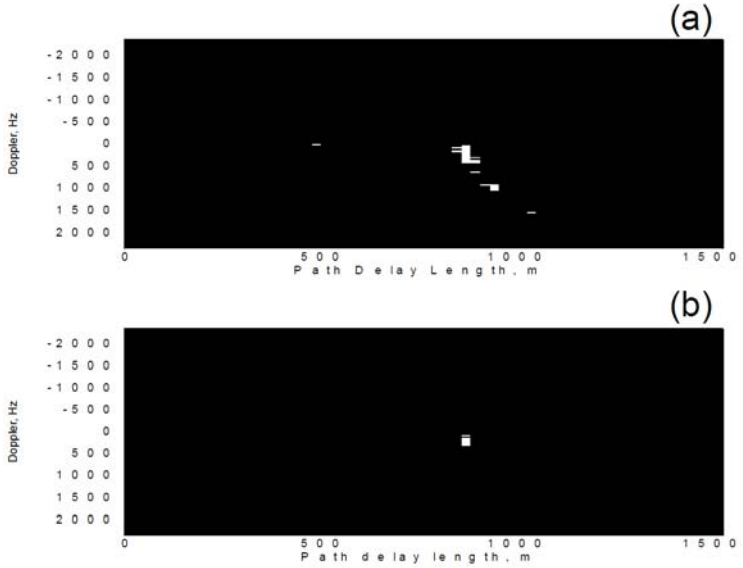

Figure 45: *CA-CFAR detection of Target A with a DVB-S Illuminator*

5.5.3.2 DVB-T detection of Target A

The data file analysed here consists of 300 frames, in which frame 100 is shown in Figure 46. There are two slow moving, closely spaced targets at the same Doppler frequency of 30 Hz and path delay lengths of 4400 m and 4600 m as indicated by the arrow. CFAR detections at this Doppler frequency are shown in Figure 47. Due to the presence of target-like signals in the set of reference data, CA-CFAR misses both targets; OS-CFAR can marginally detect the target at path delay index 187 while it misses the one at path delay index 185; only the S-CFAR can detect both targets.

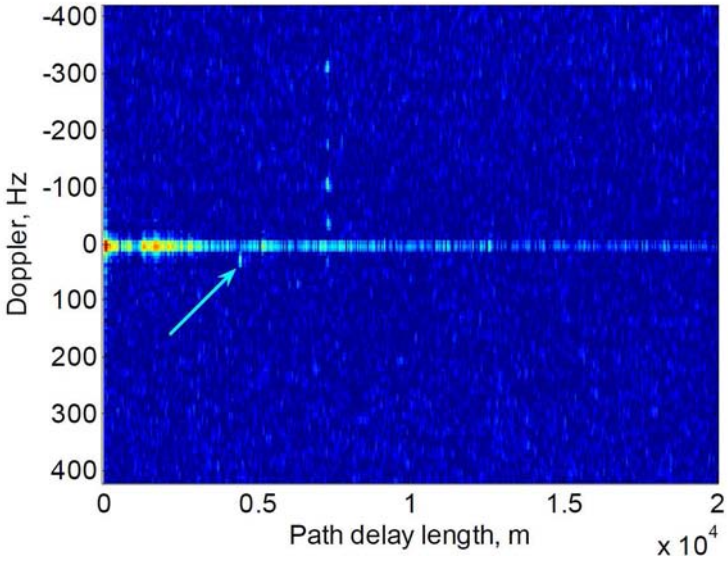

Figure 46: *Frame 100 of a DVB-T data file with two closely spaced targets path delay length 4400 m and 4600 m, Doppler=30 Hz*

5.5.3.3 DVB-T detection of Target C

The data file analysed here consists of 300 frames, in which an airborne target first appears at path delay length 4100 m, with Doppler frequency -250 Hz, and then moving with increasing speed. The CA-CFAR detector designed above is now employed to detect this target. At each cell in the path-delay-length/Doppler map, two CA-CFAR thresholding tests are performed, one in the path-delay-length dimension and one in the Doppler dimension. A detection is only confirmed if both thresholding tests are passed. The results are presented in Figure 48 which shows a clear target trajectory from path delay length 4100 m to 9700 m, with an increased Doppler from -250 Hz to -520 Hz.

CFAR detection activities in frame 200 at Doppler index 23 is shown in Figure 49. In this case, as the target is a strong 22 dB signal, it can be detected by all the three CFARs with threshold well below the signal level. CFAR detection activities in frame 41 at Doppler index 38 is shown in Figure 50. In this case, the target is a weaker 16 dB signal with signal spillover into several neighbouring range cells. Two guard cells on each side

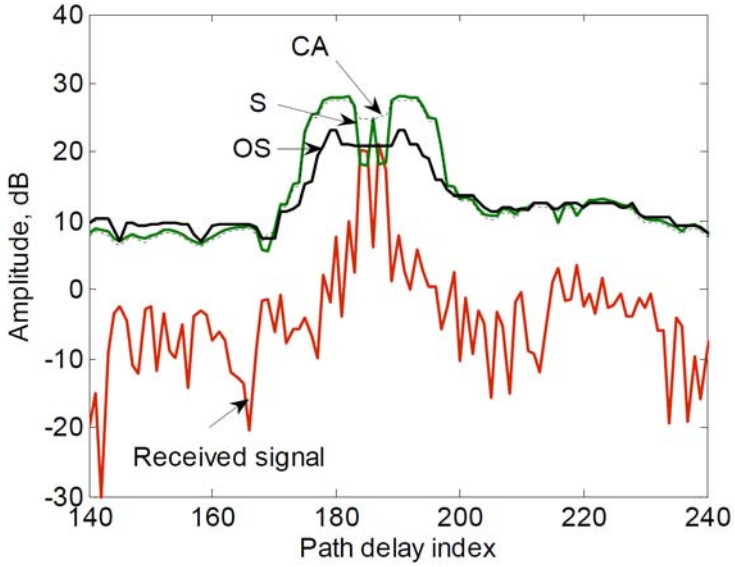

Figure 47: *CFAR detection at Doppler 30 Hz*

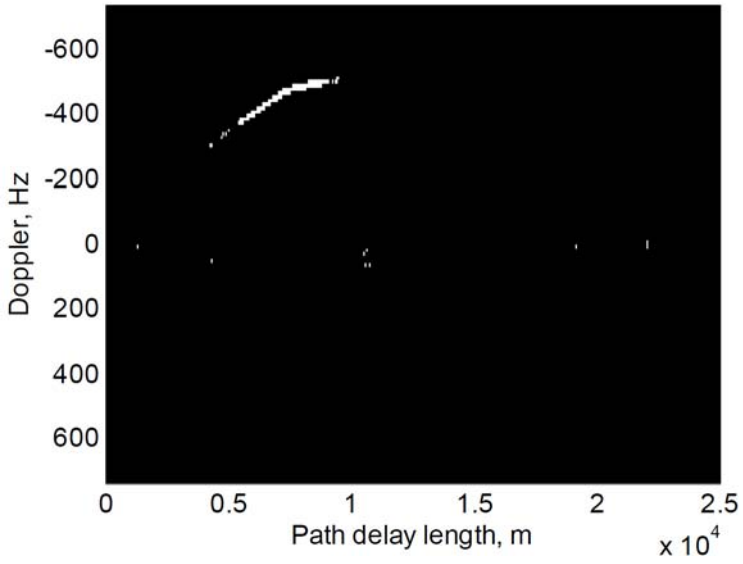

Figure 48: *CFAR detection of a clean target (Target C)*

of the test cell is now not enough to prevent signal contamination in the set of reference samples. Therefore, both the CA-CFAR and OS-CFAR marginally miss the target, while only the S-CFAR can detect the target.

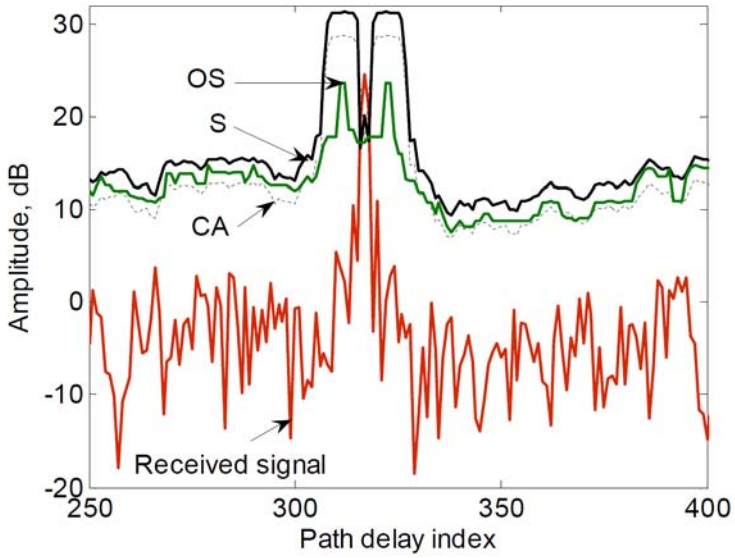

Figure 49: *CFAR detection of a clean target (Target C)*

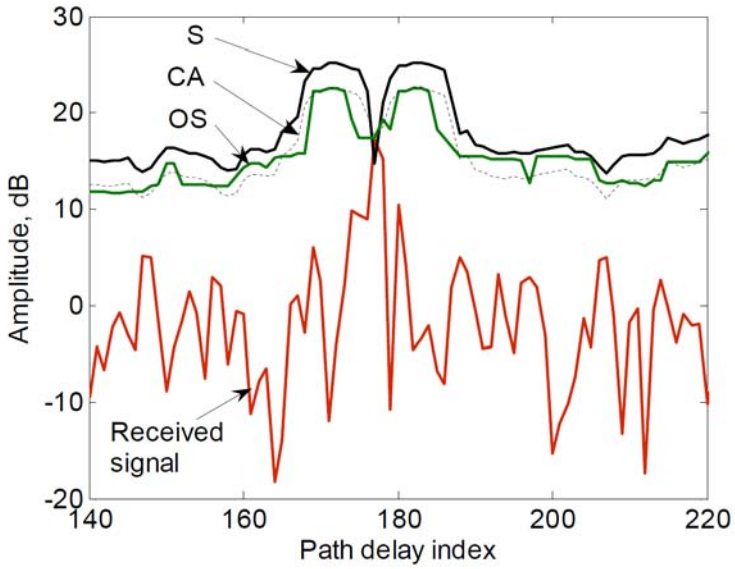

Figure 50: *CFAR detection of a clean target (Target C)*

5.5.4 CFAR Summary

In this section, CA-CFAR, OS-CFAR, and S-CFAR are employed to detect targets in the experimental data. In this application, a sliding window of 16 cells with a false alarm rate of 10^{-6} is adequate for target detection. It is evident that after CFAR detection, it is necessary to perform a further consistency check before the presence of targets can be con-

firmed. Both OS-CFAR and S-CFAR have improved robustness compared to CA-CFAR if the reference sample set is contaminated by target-like signals. In certain situations, S-CFAR is also found to be more robust than OS-CFAR in the presence of interference.

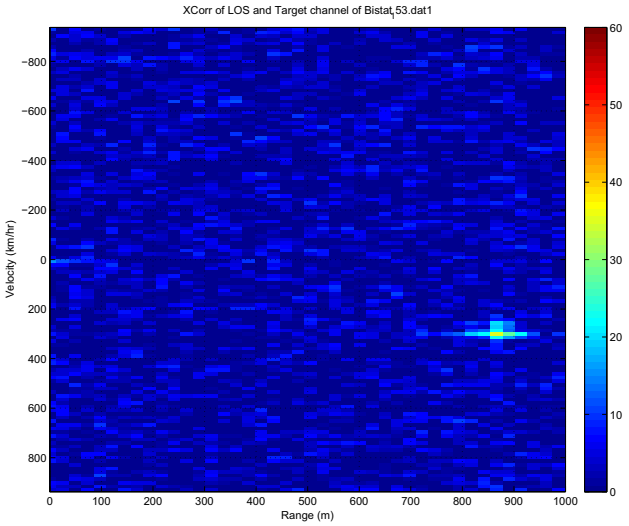

Figure 51: *Range/Doppler Surface Plot*

5.6 Coherent Processing Interval

An empirical analysis was performed to estimate the optimum coherent integration time required to achieve a maximum target SNR. Determining the optimal coherent processing interval (CPI) is contingent upon the metric that is employed. In this analysis, we shall consider peak SNR, mean SNR, and perfect integration of energy as our three metrics. The analysis was performed by taking a section of data with relatively constant target detections and varying the CPI. The SNR values were calculated for each CPI of the dataset by estimating the mean noise floor (excluding the zero Doppler and zero range lines and a window around the target), as well as the peak detection for that interval, and taking the difference. The code generated to perform this analysis may be found in Appendix C.

5.6.1 Geosynchronous Satellite (Optus C1)

The dataset used in this analysis was a three second capture of an aircraft at a path delay of just over 900 metres. A sample range-Doppler map of a 100 ms CPI from this capture can be seen in Figure 51.

The CPI was varied between 5 ms and 120 ms, predominantly in 5 ms increments. Figure 52 is a histogram plot of the mean noise floor (MNF) versus CPI. This figure shows that for each CPI the noise histogram appears to be Rayleigh distributed, as is expected, and that the noise power is increasing with CPI.

To investigate the spread of SNR values with respect to CPI a 2D histogram of the target reflected SNR versus CPI is presented in Figure 53. This figure displays the distribution of the target reflected SNR for each CPI, and shows that the overall spread of the distribution appears to be increasing with CPI.

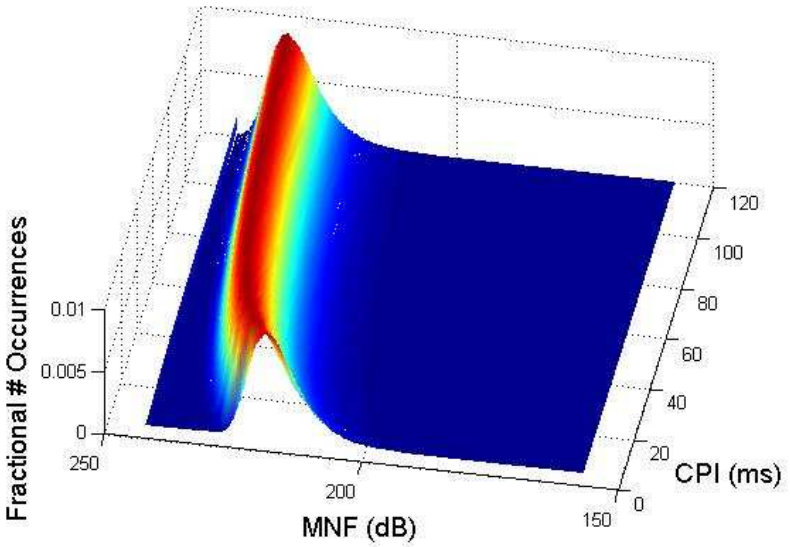

Figure 52: *Histogram of MNF vs. CPI*

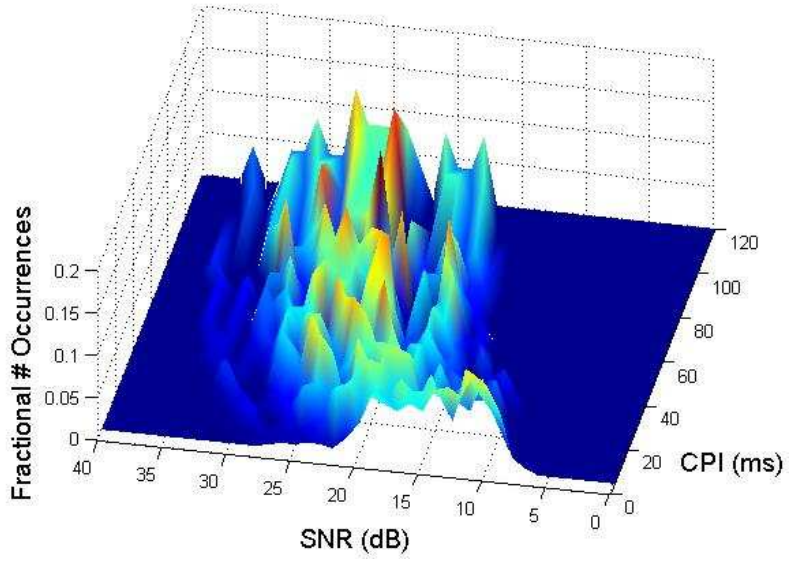

Figure 53: *Histogram of target SNR vs. CPI*

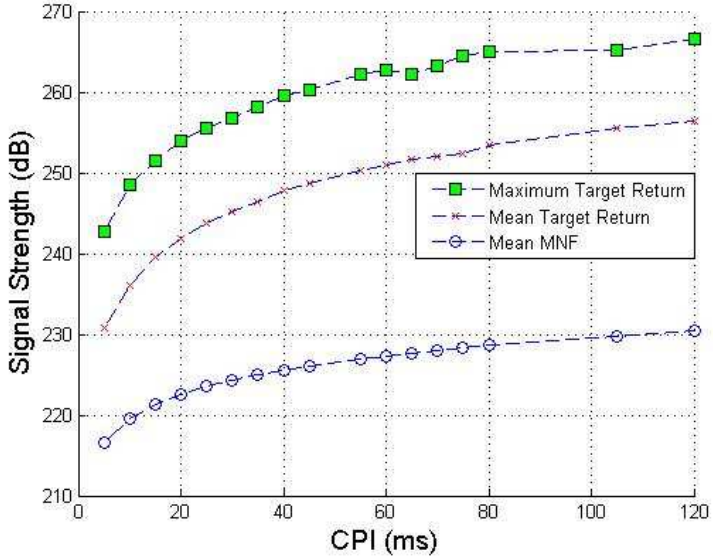

Figure 54: *Signal strength versus CPI: Target peak, target mean, and noise floor mean*

Using the data presented in Figures 52 and 53, the peak target reflected signal level, mean target reflected signal level and mean noise floor value were derived for each CPI. This information is displayed in Figure 54. As can be seen from this figure, the optimal CPI from a coherent integration standpoint (whereby the energy is integrated perfectly coherently) is approximately 40 ms.

Figure 55 displays the peak and mean SNR values and simplifies the assessment of the optimal CPI from a peak and mean SNR standpoint. Should we use the peak SNR as the metric, then a CPI of 80 ms looks to be ideal. Determining the optimal CPI based on the mean SNR is not yet possible as the mean SNR is still increasing at 120 ms, indicating that its optimal CPI has yet to be reached (although it does appear to be reaching a plateau).

It should be noted that this CPI analysis has only considered coherent integration; inclusion of incoherent summation and computational processing time will greatly influence the optimality criterion.

5.6.2 DVB-T (SBS Digital Ch 33 Mt Lofty South Australia)

A five second dataset consisting of a relatively stable detection of an aircraft at a path delay just over 5.5 km was utilised. The dataset uses a Terrestrial Digital Video Broadcast service, SBS Ch 33, as an illuminator. As the DVB-T illuminator is expected to have a higher optimum CPI (due to its longer wavelength), a five second dataset was used instead of a three second one to allow more points to be compared in the processing. A surface plot depicting range vs. Doppler for one of the CPI's can be seen in Figure 56.

The CPI was varied from 20 ms to 300 ms, again predominantly in 5 ms increments. To investigate the effects of different CPI's on the SNR and MNF a histogram plot of the SNR versus CPI and a plot of the MNF versus CPI were constructed and can be seen in Figures 57 and 58 respectively.

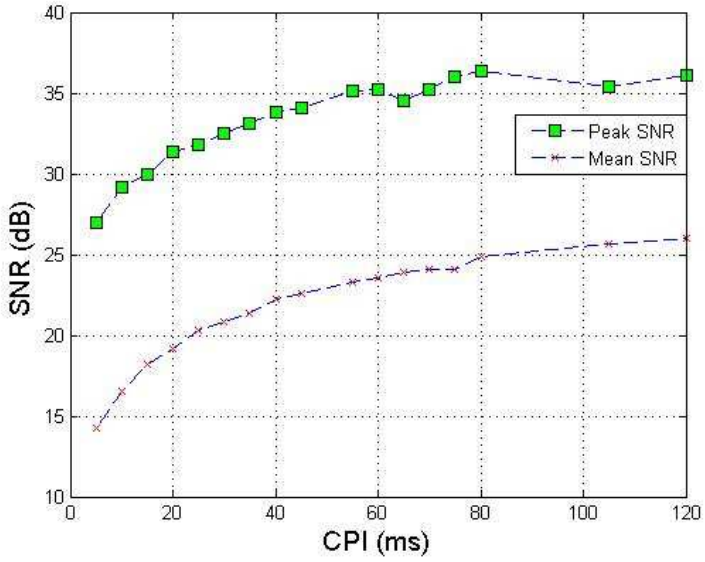

Figure 55: *Peak SNR and mean SNR versus CPI*

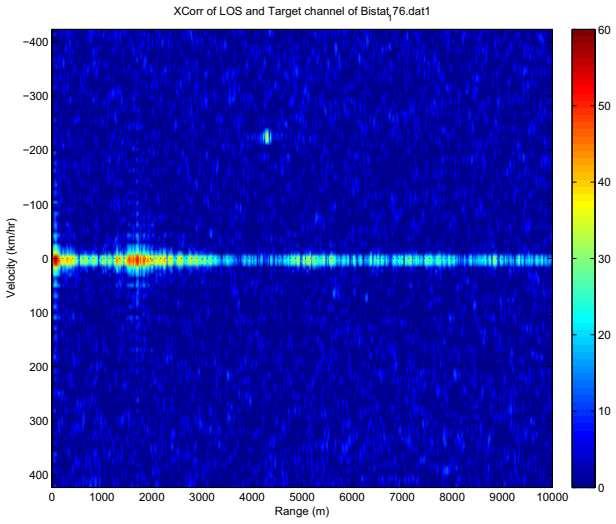

Figure 56: *Range/Doppler Surface Plot*

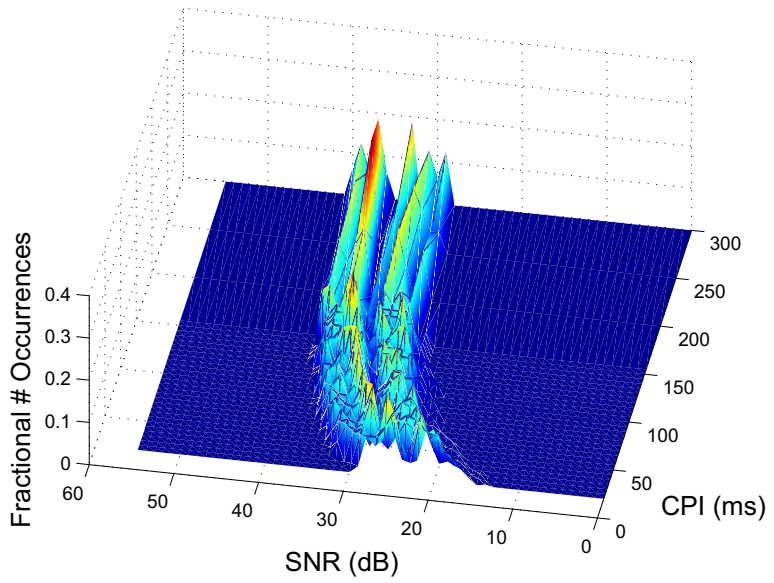

Figure 57: *Histogram of target SNR vs. CPI*

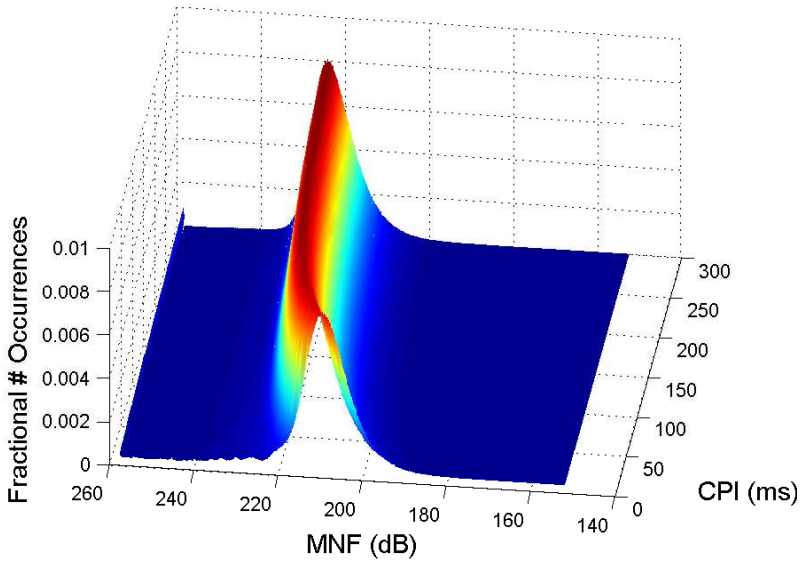

Figure 58: *Histogram of MNF vs. CPI*

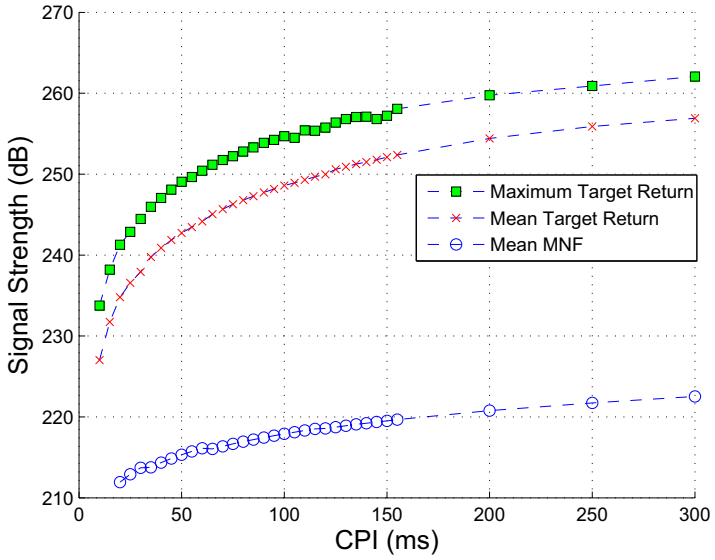

Figure 59: *Signal strength versus CPI: Target peak, target mean, and noise floor mean*

When observing the histogram plot of the MNF versus CPI, it can again be seen that for each CPI the noise histogram appears to be Rayleigh distributed and the noise power is increasing with CPI. The histogram plot of the SNR versus CPI displays the distribution of the target reflected SNR for each CPI, and indicates that the overall spread of the distribution appears to be increasing with CPI.

Using the data from both the SNR and MNF histogram plots, the peak target reflected signal level, mean target reflected signal level and mean noise floor value were derived for each CPI. This information is displayed in Figure 59. The figure indicates that the optimal CPI from a coherent integration standpoint can not be determined as the target seems to remain coherent up until the outer bounds of the CPI measurements.

Figure 60 displays the peak and mean SNR values and simplifies the assessment of the optimal CPI from a peak and mean SNR standpoint. If the peak SNR is utilised as the metric, then a CPI of 150 ms is ideal. The mean SNR gives further evidence to this CPI being the optimal CPI for the SNR metric, as the mean SNR starts to plateau after 150 ms. It should be noted that this CPI analysis has only considered coherent integration; inclusion of incoherent summation and computational processing time will greatly influence the optimality criterion.

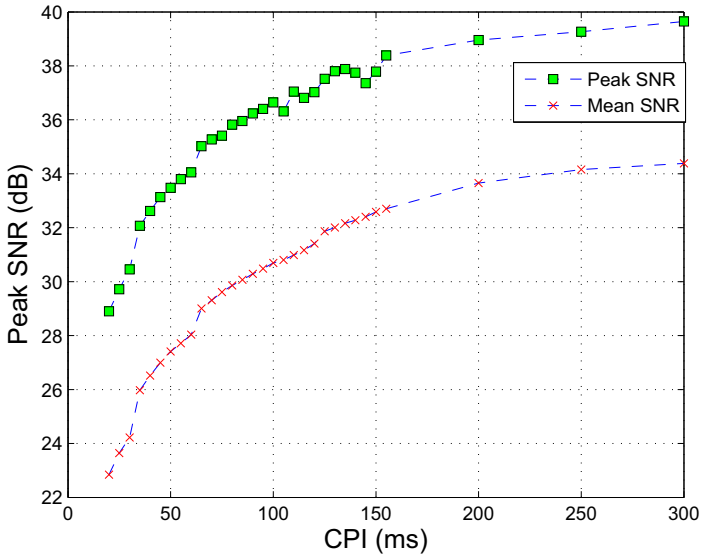

Figure 60: *Peak SNR and mean SNR versus CPI*

6 Potential Application Areas for PCL

Whilst still preliminary in nature, the results presented in this report begin to indicate a level of capability for PCL systems. Realising this capability level would give rise to a number of application areas that may capitalise on the advantages provided by PCL systems. Some examples of potential application areas are:

- Ground based surveillance of aircraft over metropolitan regions using terrestrial TV transmissions
- Short range ground based surveillance of aircraft using geosynchronous satellites
- Short range ground based surveillance of aircraft using GNSS satellites (viability yet to be determined)
- Maritime target detection using either terrestrial or satellite transmitters
- Passive ISAR imaging using geosynchronous satellites
- Passive SAR imaging using GNSS satellites and a stationary or dynamic receiver
- Passive SAR imaging using geosynchronous satellites and a dynamic receiver
- Passive airborne surveillance SAR over metropolitan regions using DVB-T

This list incorporates a number of areas that would be relatively simple to implement, such as the ground based surveillance of aircraft over metropolitan regions using terrestrial TV transmissions, as well as others that are much more ambitious (such as the passive SAR/ISAR imaging using satellite illuminators for example), and correspondingly, would entail a higher degree of technical risk in development and implementation.

In order for a number of these application areas to be realised, extensive supporting research must be carried out. The following list presents some insights into the types of supporting research activities that would be required to realistically deploy a PCL system in, for example, the maritime target detection application area.

- Maritime bistatic clutter measurements (for each transmitter and with a representative geometrical variety)
- Bistatic target data collection (again, for each transmitter and with a representative geometrical variety)
- Development of parametric detection methods of targets and clutter
- Development of display tools for bistatic data

7 Future Work

Even though the research results discussed in this report are still preliminary in nature, the key outcomes of this research, to date, may be separated into two distinct groups: Things that we do know and/or have experimentally demonstrated, and things that we do not know and/or are yet to experimentally verify. Summaries of these groups are provided in Sections 7.1 and 7.2. A large part of the future research to be completed in this area will be focused on answering the questions raised in Section 7.2, predominantly using the experimental research directions discussed in Section 7.3, and the analytical and signal processing research indicated in Section 7.4.

7.1 Things that We Do Know and/or Have Experimentally De-monstrated

In the research conducted to date we have demonstrated that:

- Simple signal processing (i.e. cross-correlation, Fourier transforming and Doppler filtering) on the DVB-T and DVB-S signals provides enough signal processing gain to detect secondary reflections from these illuminators
- Aircraft and terrestrial automotive targets can be detected and tracked from their skin echoes using DVB-T and DVB-S signals
- Unmodified terrestrial analogue TV signals provide good Doppler resolution but poor range resolution, but have a higher power than the DVB-T signals (approximately 6 dB)
- "Alias and Integrate" does not provide a signal processing gain over the standard approach, and in fact, may degrade performance.

7.2 Things that We Do Not Know and/or are Yet to Experimentally Verify

The future directions that this research will take, will largely be driven by the following questions:

- What are the maximum detection ranges of the DVB-T and DVB-S two channel systems using both standard and advanced signal processing?
- What are the maximum detection ranges of the multichannel systems?
- How can the system be calibrated?
- What is the optimal incoherent integration period?
- What is the optimal bistatic angle/aspect angle for detecting aircraft (i.e. for maximising the target's RCS)?

- What is the impact of the terrestrial TV transmitter's elevation beam pattern on the detectability of aircraft?

- What angular precision in azimuth and elevation can be achieved with either an interferometer or a phased array?

- What gain in the output of the cross-correlation can be achieved by demodulating, applying FEC and remodulating the reference signal (c.f. Section 5.2.2)?

7.3 Future Experimental Research Directions

Directions that future research into this area include:

1. Multi-element receivers in order to allow beamforming on receive - including linear and 2D arrays (this work could be supported by the antenna array trailer that is being designed and may be built by SES)

2. Multistatic system analysis using two (or more) geosynchronous satellite illuminators

3. Multifrequency bistatic system analysis using both the analogue and digital terrestrial TV signals

4. Coordinated experimental data collection with the Royal Australian Air Force (RAAF) - this would provide target truth data for calibration and comparison

5. Determine what SNR improvement can be achieved by using better quality LNBFs or Masthead amplifiers

7.4 Future Analytical and Signal Processing Directions

Research directions that this research would support and, in turn, would be supported by include:

1. Further development of tracking algorithms that can exploit bistatic data

2. Further development of CFAR and/or other detection algorithms that are specific to the collected datasets

3. Waveform diversity and scheduling research

4. Bistatic Space-Time Adaptive Processing (STAP) / Terrain Scatterer Interference (TSI) research

8 Conclusion

In this report EWRD's new illuminator of opportunity bistatic radar research project has been introduced. Several transmitters were identified for illuminator of opportunity research, power budgets and waveform ambiguity analyses provided, and preliminary target detections using a terrestrial TV transmitter and geosynchronous satellite presented. The applicability of several CFAR and Track Before Detect algorithms were also demonstrated via a proof of concept test. Sections 7.1 and 7.2 summarize what has and has yet to be experimentally verified, and also begins to elucidate some of the future research directions of this project.

Acknowledgements

The authors would like to gratefully acknowledge the assistance and efforts of numerous individuals whose help greatly improved this work. In no particular order, the authors would like to thank: David Merrett, Ashley Summers, Sam Davey, Mark Rutten, Paul Berry, Desmond Yau, Ron Fullgrabe, Jamie Carter, Dennis Sachse, Hedley Hansen, Scott Capon, Andrew Shaw, Stephen Searle, Vaughan Thomas, Ian May, Jayasanka Piyaratna, David Dempsey and Ian Chant (may he rest in peace).

References

1. Cherniakov, M., Kubik, K. & Nezlin, D. (2000) Bistatic synthetic aperture radar with non-cooperative leos based transmitter, *IEEE 2000 International Geoscience and Remote Sensing Symposium* , 7 vol.(clvi+3242).

2. Baniak, J., Baker, D. G., Cunningham, A. & Martin, L. (2008) Silent sentry passive surveillance. URL – `www.dtic.mil/ndia/jaws/sentry.pdf`.

3. Roke Manor (2002) BAE SYSTEMS and Roke Manor Research Team to Develop Revolutionary Cellphone Radar, website. URL – `http://www.roke.co.uk/press/38.php`. last checked = 15/10/2008.

4. Ringer, M. A., Frazer, G. J. & Anderson, S. J. (1999) *Waveform Analysis of Transmitters of Opportunity for Passive Radar*, Technical report, Defence Science and Technology Organisation.

5. Griffiths, H. D. & Long, N. (1986) Television-based bistatic radar, *IEE Proceedings* **133, Pt.F**(7), 649–657.

6. Griffiths, H. D. & Baker, C. J. (2005) Measurement and analysis of ambiguity functions of passive radar transmissions, *IEEE 2005 International Radar Conference* , 321–325.

7. Howland, P. (1999) Target tracking using television-based bistatic radar, *IEE Proceedings-Radar, Sonar and Navigation* **146**(3), 166–174.

8. Howland, P. (2005) Editorial - passive radar systems, *IEE Proceedings-Radar, Sonar and Navigation* **152**(3), 105–6.

9. Griffiths, H. D., Baker, C. J. & Papoutsis, I. (2005) Passive coherent location radar systems. part 2: Waveform properties, *IEE Proceedings-Radar, Sonar and Navigation* **152**(3), 160–168.

10. Griffiths, H. D. & Baker, C. J. (2005) Passive coherent location radar systems. part 1: performance prediction, *IEE Proceedings-Radar, Sonar and Navigation* **152**(3), 153–159.

11. Howland, P., Masksimiuk, D. & Reitsma, G. (2005) Fm radio based bistatic radar, *IEE Proceedings-Radar, Sonar and Navigation* **152**(3), 107–115.

12. Taşdelen, A. & Kőymen, H. (2006) Range resolution improvement in passive coherent location radar systems using multiple fm radio channels, *The Institution of Engineering and Technology Forum on Waveform Diversity and Design in Communications, Radar and Sonar, 2006* , 23–31.

13. Palmer, J., Merrett, D., Palumbo, S., Piyaratna, J., Capon, S. & Hansen, H. (2008) Illuminator of opportunity bistatic radar research at dsto, *IEEE 2008 International Radar Conference* , .

14. Zhiwen, G., Ran, T., Yongfeng, M. & Tao, S. (2006) Dvb-t signal cross-ambiguity functions improvement for passive radar, *International Conference on Radar 2006. CIE '06'* , 1–4.

15. Griffiths, H., Garnett, A., Baker, C. & Keaveney, S. (1992) Bistatic radar using satellite-borne illuminators of opportunity, *International Conference on Radar 92* , 276–279.

16. Griffiths, H., Baker, C., Baubert, J., Kitchen, N. & Treagust, M. (2002) Bistatic radar using satellite-borne illuminators, *International Conference on Radar 2002* , 1–5.

17. Kubica, M., Kubica, V., Neyt, X., Raout, J., Roques, S. & Acheroy, M. (2006) Optimum target detection using illuminators of opportunity, *IEEE Conference on Radar 2006* , 417–424.

18. Thomas, J., Griffiths, H. & Baker, C. (2006) Ambiguity function analysis of digital radio mondiale signals for hf passive bistatic radar, *Electronic Letters* **42**(25), 1482–1483.

19. Lok, J. (October, 2007) You're on the air - passive radar uses fm signals to defeat stealth, *Defence Technology International* **Vol. 1, No. 7**, 32.

20. Thales (2008) Solutions for air traffic management today and tomorrow. URL– `http://www.thalesraytheon.com/press-and-media.html`.

21. Thales (2008) Homeland alerter 100, http://www.thalesraytheon.com/en/business-and-products/products/radars/passive-radars/homeland-alerter-100.html. lastchecked = 15/10/2008.

22. Thales (2008) Ground alerter 10, http://www.thalesgroup.com/eurosatory2008/standthales3.html. last checked: 15/10/2008.

23. Thales (2008) Solutions: Ground alerter 10, http://www.thalesgroup.com/markets/Activities/Product-page.html?url=/Activities/Air-Defence/Radar-and-Sensors.html?locale=EN-gb\&link=39266614-6159-7A38-326B-38027D7E5E06:central\&locale=EN-gb\&Title=Ground+Alerter+10\&dis=1\&marketId=0A50731B-644D-1E7E-3C5B-150646382719\&type=Market. last checked: 15/10/2008.

24. Trinkle, M. & Cooke, P. (2008) *Experimental Equipment Development for GPS Bistatic Radar - Parabolic Reflector Trough Development and Testing*, Dsto task report for task 2.16, DSTO.

25. Glennon, E., Dempster, A. & C., R. (2006) Feasibility of air target detection using gps as a bistatic radar, *Journal of Global Positioning Systems* **5**(1-2), .

26. Optus & Singtel (2007) Optus - about optus - satellite network, http://www.optus.com.au/portal/site/aboutoptus/menuitem.cfa0247099a6f722d0b61a108c8ac7a0/?vgnextoid=acf9d1475accc010VgnVCM10000029867c0aRCRD. last checked: 15/10/2008.

27. ACMA (2007) *Section 8 - Television - Area Served*, Technical report, Australian Communication and Media Authority. URL– http://www.acma.gov.au/webwr/_assets/main/lib100059/tv_8.pdf.

28. Skolnik, M. I. (2008) *Radar handbook*, 3rd edition edn, McGraw-Hill, New York.

29. Davey, S. J., Rutten, M. G. & Cheung, B. (2007) A comparison of detection performance for several track-before-detect algorithms, *EURASIP Journal on Advances in Signal Processing* **2008**, 10.

30. Berry, P. E. & Yau, D. (2008) *Bayesian Track-Before-Detect - Analysis and Implementation Issues*, Technical report, Defence Science and Technology Organisation.

31. Koch, V. & Westphal, R. (1995) New approach to a multistatic passive radar sensor for air/space defense, *IEEE Aerospace and Electronic Systems Magazine* **10**(11), 24–32.

32. Cherniakov, M., Nezlin, D. & Kubik, K. (2002) Air target detection via bistatic radar based on leos communication signals, *IEE Proceedings-Radar, Sonar and Navigation* **149**(1), 33–8.

33. Skolnik, M. I. (2001) *Introduction to Radar Systems*, 3nd edition edn, McGraw-Hill Book Company, USA.

34. Finn, H. & Johnson, R. (1968) Adaptive detection mode with threshold control as a function of spatially sampled clutter level estimate, *RCA Review* **29**(3), 414–464.

35. Gandhi, P. & Kassam, S. (1988) Analysis of cfar processors in nonhomogeneous background, *IEEE Transactions on Aerospace and Electronic Systems* **24**(4), 427–445.

36. Cao, T. (2008) Constant false-alarm rate algorithm based on test cell information, *IEE Proceedings-Radar, Sonar and Navigation* **2**(3), 200–213.

Appendix A Power Budget Studies Code

- Note: All code displayed in Appendix A, B and C was written in MATLAB, Version number 7.2.0.283 (R2006a)

Geosynchronous Satellite Power Budget

```
clear all
% Power Budget Link Calculator for Bistatic Radar for Ku Geo Satellite
c = 3e8; % Speed of Light
f = 12.5e9; %  Frequency
k = 1.38e-23; % Boltzman's Constant
RCS = 20; % in m^2
T_eff = 580; %From Glennon Paper
B = 12.5e6;
SNRmindB = 13;
SNRmin = 10^(SNRmindB/10);
% Tau_coh = 10e-3:1e-3:1000e-3;
Tau_coh = 100e-3;
L_sp = 2.11; % From Glennon Paper
lambda = c/f; % Wavelength
G_Array = 15;
Gr_dB = 38; % Gain of receiver in dB

disp(' ')
disp(' ')
% EIRP_dB = 40:51; %dBW Range between 40 and 51 dBW
EIRP_dB = 51; %dBW Range between 40 and 51 dBW
EIRP = 10.^(EIRP_dB/10);

% Pt = 36; % Transmit power of GPS satellite in Watts - UNVERIFIED
% Gt =

R_Direct = 37341880; % Average distance from Earth ~36000km

% SFD_dB = -88; % dBW/m2 - Taken from www.optus.com.au - Range listed as
% -78 dBW/m2 -> -98 dBW/m2
%
% SFD = 10^(SFD_dB/10);
% S_direct = SFD;

% Gt = SFD*4*pi*R_Direct^2/Pt; % Transmitter gain given current parameters
% Gt_dB = 10*log10(Gt);

% EIRP = SFD*4*pi*R_Direct^2;
```

```
% EIRP = Pt*Gt; % GPS EIRP - some estimates (starlab paper)
% have it at 29.4dBW

% EIRP_dB = 10*log10(EIRP);

pathLoss_dB = 10*log10(4*pi*R_Direct^2);

S_direct = EIRP/(4*pi*R_Direct^2);  % LOS PFD
S_dir_dB = 10*log10(S_direct);

% disp(['S_dir_dB is ', num2str(S_dir_dB), ', should be -78 -> -98dBW/m^2'])

% AeT = lambda^2*Gt/(4*pi); % Effective Area of Transmitter

Gr = 10^(Gr_dB/10);

N_0 = k*T_eff*B;  % Check the Bandwidth value vs. signal Bandwidth VALUE!!!!

AeR = lambda^2*Gr/(4*pi);

B_op = 1./Tau_coh;
G_sp = B./B_op;
%%
for ii = 1:length(S_direct)
R_t(:,ii) = sqrt(S_direct(ii)*RCS*AeR*G_sp./(SNRmin*N_0*L_sp*4*pi));
end

figure(1)
plot(R_t, Tau_coh)
legend([num2str(EIRP_dB.')])

xlabel('Range (m)')
ylabel('Coherent Integration Time (sec)')
%%
% disp(['Coherent Integration time is ', num2str(Tau_coh), ' s'])
% disp(' ')
disp(['Maximum single element detection range is ', num2str(R_t), ' m'])

for ii = 1:length(S_direct)
R_t_Array(:,ii) = sqrt(S_direct(ii)*RCS*AeR*G_sp.*G_Array/...
(SNRmin*N_0*L_sp*4*pi));
end
disp(' ')
disp(['Maximum ', num2str(G_Array), ' element array detection range is ',...
num2str(R_t_Array), ' m'])

figure(2)
```

```
plot(R_t_Array, Tau_coh)
legend([num2str(EIRP_dB.')])

xlabel('Range (m)')
ylabel('Coherent Integration Time (sec)')
```

Terrestrial TV Power Budget

```
clear all

% Power Budget Link Calculator for Bistatic Radar for Terrestrial TV

c = 3e8; % Speed of Light
f = 0.5645e9; %  Frequency
k = 1.38e-23; % Boltzman's Constant
RCS = 20; % in m^2
T_eff = 344; %From Glennon Paper
B = 12.5e6;
% SNRmin = 20.1051;
SNRmindB = 13;
SNRmin = 10^(SNRmindB/10);
Tau_coh = 0.4e-3;
L_sp = 2.11; % From Glennon Paper
lambda = c/f; % Wavelength
G_Array = 15;
disp(' ')
disp(' ')

% Pt = 200e3; % Transmit power of TV Transmitter Watts
% Gt = 10; % Gain of TV Transmitter - UNVERIFIED

R_Direct = 31280; % Mt Lofty to RAAF Base

% R_Direct = 29170; % Mt Lofty to STF

% R_Direct = 28260; % Mt Lofty to 180 Labs

% Gt = SFD*4*pi*R_Direct^2/Pt; % Transmitter gain given current parameters
% Gt_dB = 10*log10(Gt);

EIRP = 200e3; % As per Ian May's document - ASSUMPTION: 200kW is ERP...

EIRP_dB = 10*log10(EIRP);

% R_Total = R_1 + R_t;
```

```
SFD = EIRP/(4*pi*R_Direct^2);

SFD_dB = 10*log10(SFD); % dBW/m2

S_direct = EIRP/(4*pi*R_Direct^2);  % LOS SFD

pathLoss_dB = 10*log10(4*pi*R_Direct^2);

% S_direct = EIRP/(4*pi*R_Direct^2);  % LOS SFD
% S_dir_dB = 10*log10(S_direct);
%
% disp(['S_dir_dB is ', num2str(S_dir_dB), ', should be ~-88dBW/m^2'])

% AeT = lambda^2*Gt/(4*pi); % Effective Area of Transmitter

Gr_dB = 13; % Gain of receiver in dB
Gr = 10^(Gr_dB/10);

N_0 = k*T_eff*B;  % Check the Bandwidth value vs. signal Bandwidth VALUE!!!!

AeR = lambda^2*Gr/(4*pi);

B_op = 1/Tau_coh;
% G_sp = B/B_op;
G_sp = 1;

R_TotalProd = sqrt(EIRP*RCS*AeR*G_sp/(SNRmin*N_0*L_sp*(4*pi)^2));

R_t = sqrt(R_TotalProd);

disp(['Maximum single element detection range is ', num2str(R_t), ' m'])

R_TotalProd_Array = sqrt(EIRP*RCS*AeR*G_sp*G_Array/...
(SNRmin*N_0*L_sp*(4*pi)^2));

R_t_Array = sqrt(R_TotalProd_Array);
disp(' ')
disp(['Maximum 15 element array detection range is ',...
num2str(R_t_Array), ' m'])
```

GPS Power Budget

```
clear all
```

```
% Power Budget Link Calculator for Bistatic Radar for GPS

c = 3e8; % Speed of Light
f = 1.57542e9; % GPS L2 Frequency
k = 1.38e-23; % Boltzman's Constant
RCS = 20; % in m^2
T_eff = 344; %From Glennon Paper
B = 2.046e6;
% SNRmin = 20.1051;
SNRmindB = 13;
SNRmin = 10^(SNRmindB/10);
Tau_coh = 1;
L_sp = 2.11; % From Glennon
lambda = c/f; % GPS Wavelength
G_Array = 15;
disp(' ')
disp(' ')

Pt = 36; % Transmit power of GPS satellite in Watts - UNVERIFIED
% Gt =

R_Direct = 20181000; % Average distance from Earth 20181km

SFD_dB = -134; % dBW/m2 - Taken from Glennon Paper

SFD = 10^(SFD_dB/10);

Gt = SFD*4*pi*R_Direct^2/Pt; % Transmitter gain given current parameters
Gt_dB = 10*log10(Gt);

EIRP = Pt*Gt; % GPS EIRP - some estimates (starlab paper) have it at 29.4dBW

EIRP_dB = 10*log10(EIRP);

pathLoss_dB = 10*log10(4*pi*R_Direct^2);

S_direct = EIRP/(4*pi*R_Direct^2);  % LOS SFD
S_dir_dB = 10*log10(S_direct);

disp(['S_dir_dB is ', num2str(S_dir_dB), ', should be ~134dBW/m^2'])
disp(' ')

AeT = lambda^2*Gt/(4*pi); % Effective Area of Transmitter

Gr_dB = 17; % Gain of receiver in dB
Gr = 10^(Gr_dB/10);
```

```
N_0 = k*T_eff*B;

AeR = lambda^2*Gr/(4*pi);

B_op = 1/Tau_coh;
G_sp = B/B_op;

R_t = sqrt(S_direct*RCS*AeR*G_sp/(SNRmin*N_0*L_sp*4*pi));

SNR239 = S_direct*RCS*lambda^2*31.62/(4*pi)*G_sp/(N_0*L_sp*4*pi*239^2);
SNR2510 = S_direct*RCS*lambda^2*3481/(4*pi)*G_sp/(N_0*L_sp*4*pi*2510^2);

disp(['Maximum single element detection range is ', num2str(R_t), ' m'])

R_t_Array = sqrt(S_direct*RCS*AeR*G_sp*G_Array/(SNRmin*N_0*L_sp*4*pi));
disp(' ')
disp(['Maximum 15 element array detection range is ',...
num2str(R_t_Array), ' m'])
```

Appendix B PCL Processing Code

```
function IOO_Dopp_bulkProc_Sdata(filename, Fc, tau_coh,...
velocity, minUnamRange)

warning off all

f_s = 12.5e6;
T_s = 1/f_s;
c = 3e8;
B = 12.5e6;
fftLength = 128;
resn = c/B;
kaiserBeta = 3.5;

maxlags = ceil(minUnamRange/resn);
if (tau_coh/T_s)<=maxlags
    maxlags = tau_coh/T_s;
end

vel = velocity*1000/(60*60); % velocity in m/s
Dopp_max = 2*vel*(Fc)/c;
tau_corr = 1/(2*Dopp_max);
corrSumNo = ceil(tau_coh/tau_corr);

tau_corr = tau_coh/corrSumNo;

if isunix
    Fullfilename = ['/data/pcldata/', filename];
    Savefilename = ['/data/pcldata/Matlab_data/', filename(1:end-5), '_'];
else
    Fullfilename = ['P:\pcldata\', filename];
    Savefilename = ['P:\pcldata\Matlab_data\', filename(1:end-5), '_'];
end

% maxmem_samps = (2^31-64)/64;
maxmem_samps = 3*12.5e6; %3s
file_det = dir(Fullfilename);
file_samps = (file_det.bytes-1024)/16;
file_time = file_samps/12.5e6;
if file_samps > maxmem_samps
    num_maps = ceil(file_samps/maxmem_samps);
else
    num_maps = 1;
end
disp([num2str(num_maps) ' to process...'])
start_time = 0;
```

```
stop_time = maxmem_samps/12.5e6;

% initialise ffts
fftACF1 = [];
fftACF2 = [];
fftXC1 = [];
fftXC2 = [];
tic
for map_cnt = 1:num_maps
    disp(['Processing map ' num2str(map_cnt) '/' num2str(num_maps) ': ',...
     num2str(stop_time-start_time) 's'])
    [h,d] = Readfile_NoSm_Skip_v2(Fullfilename,start_time,stop_time);

    d1 = d(:,1);
    d2 = d(:,2);
%     d3 = d(:,3);
    d4 = d(:,4);
    clear d
    dLength = length(d2);

    corr_length = tau_corr/T_s;
    loopNo = floor(dLength/(corr_length*corrSumNo));
    disp([num2str(loopNo) ' loops'])
    for ii = 1:loopNo
        for kk = 1:corrSumNo
            segmentIndexStart = (kk-1+(ii-1)*corrSumNo)*corr_length+1;
            segmentIndexStop = (kk+(ii-1)*corrSumNo)*corr_length;
            ACF1(kk,:)=xcorr_simo(d1(segmentIndexStart:segmentIndexStop),...
             d1(segmentIndexStart:segmentIndexStop), maxlags);
            ACF2(kk,:)=xcorr_simo(d2(segmentIndexStart:segmentIndexStop),...
             d2(segmentIndexStart:segmentIndexStop), maxlags);
            XC1(kk,:)=xcorr_simo(d4(segmentIndexStart:segmentIndexStop),...
             d1(segmentIndexStart:segmentIndexStop), maxlags);
            XC2(kk,:)=xcorr_simo(d4(segmentIndexStart:segmentIndexStop),...
             d2(segmentIndexStart:segmentIndexStop), maxlags);
            % Note: xcorr_simo is a modified version of the xcorr function
            % that only outputs the positive delay side of the cross
            % correlation
        end
        if ii == 1
            ACFSize = size(ACF1);
            wDopp = kaiser(ACFSize(1), kaiserBeta);
            WDopp = repmat(wDopp, 1, ACFSize(2));
            WRange =ones(ACFSize(1),ACFSize(2));
        end
        fftACF1t(:,:,ii) = fftshift(fft(WRange.*WDopp.*ACF1,fftLength),1);
        fftACF2t(:,:,ii) = fftshift(fft(WRange.*WDopp.*ACF2,fftLength),1);
```

```
        fftXC1t(:,:,ii) = fftshift(fft(WRange.*WDopp.*XC1,fftLength),1);
        fftXC2t(:,:,ii) = fftshift(fft(WRange.*WDopp.*XC2,fftLength),1);
        if rem(ii,5) == 0
            disp(num2str(ii))
        end
    end
    fftACF1 = cat(3,fftACF1,fftACF1t);
    fftACF2 = cat(3,fftACF2,fftACF2t);
    fftXC1 = cat(3,fftXC1,fftXC1t);
    fftXC2 = cat(3,fftXC2,fftXC2t);
    clear ACF1 ACF2 XC1 XC2 fftACF1t fftACF2t fftXC1t fftXC2t d1 d2 d3 d4
    start_time = (map_cnt*maxmem_samps)/12.5e6;
    stop_time = (map_cnt+1)*maxmem_samps/12.5e6;
    if stop_time > file_time
        stop_time = file_time;
    end
end

% set up params structure
DoppLinspace = linspace(-1/(tau_corr*2),1/(tau_corr*2),...
length(fftXC1(:,1,1)));
xTickMark = 1:resn:round(length(fftXC1(1,:,1)))*resn-1;
params.filename = filename;
params.Fc = Fc;
params.tau_coh = tau_coh;
params.velocity = velocity;
params.minUnamRange = minUnamRange;
params.f_s = f_s;
params.fftLength = fftLength;
params.DoppLinspace = DoppLinspace;
params.xTickMark = xTickMark;

% save
ch_info = 'ACF of Ch1';
disp('Saving data...')
save([Savefilename 'fftACF1.mat'],'fftACF1', 'params', 'ch_info');
ch_info = 'ACF of Ch2';
save([Savefilename 'fftACF2.mat'],'fftACF2', 'params', 'ch_info');
ch_info = 'XC of Ch4 & Ch1';
save([Savefilename 'fftXC1.mat'],'fftXC1', 'params', 'ch_info');
ch_info = 'XC of Ch4 & Ch2';
save([Savefilename 'fftXC2.mat'],'fftXC2', 'params', 'ch_info');

disp('Finished.')
t = toc/60;
disp(['Elapsed time is ' num2str(t) ' minutes.'])
```

Appendix C Coherent Processing Interval Code

```
close all
clear all
warning off all

read_length = 5; % Data to read in seconds
filename = 'Bistat_176.dat1';
readSkipTime = 3; %Start point in

f_s = 12.5e6; %  Sampling Frequency
T_s = 1/f_s; %Sampling Time
c = 3e8;    % Speed of light
B = 12.5e6; %Bandwidth
Fc = 564.5e6; %Centre Frequency
velocity = 400; %Velocity km/hr
velResn = 0.5; % velocity resolution in wavelengths
Beta = 45; %degrees
fftLength = 128;
lambda = c/Fc; %Wavelength
resn = c/B;
minUnamRange = 10000; % minimum unambiguous range in metres
kaiserBeta = 3.5; %Kaiser window beta parameter
%max no. of lags for x-correlation
maxlags = ceil(minUnamRange/resn);

n = gcf;
if n == 1
    n = 0;
end
tic

vel = velocity*1000/(60*60); % velocity in m/s
Dopp_max = 2*vel*(Fc)/c; %Maximum Doppler
noOfReadSamplesToSkip = round(readSkipTime*f_s);

Fullfilename = ['/data/pcldata/', filename];
read_samples = read_length*f_s;
%function to read in data
[h,d] = Readfile_NoSm_Skip_v2(Fullfilename,readSkipTime,...
readSkipTime+read_length);

d1 = d(:,1);
d2 = d(:,2);
d3 = d(:,3);
d4 = d(:,4);
clear d
```

```
dLength = length(d1)+1;

%%
jj = 0;
tau_coh_max=0.200; %Max Coherent processing interval to loop to

for count = 0.02:0.01:tau_coh_max

    corrSumNo = ceil(tau_coh/tau_corr);
    tau_corr = tau_coh/corrSumNo;
    corr_length = tau_corr/T_s;
    loopNo = floor(dLength/(corr_length*corrSumNo));

    for ii = 1:loopNo
        %cross correlation process
        for kk = 1:corrSumNo
            segmentIndexStart = (kk-1+(ii-1)*corrSumNo)*corr_length+1;
            segmentIndexStop = (kk+(ii-1)*corrSumNo)*corr_length;
            ACF(kk,:) = xcorr_simo(d1(segmentIndexStart:segmentIndexStop)...
             ,d1(segmentIndexStart:segmentIndexStop), maxlags);
            XC(kk,:) = xcorr_simo(d3(segmentIndexStart:segmentIndexStop)...
             ,d1(segmentIndexStart:segmentIndexStop), maxlags);
        end
        if ii == 1
            ACFSize = size(ACF);
            w = kaiser(ACFSize(1), kaiserBeta);
            W = repmat(w, 1, ACFSize(2));
        end
        fftXC = fftshift(fft(W.*XC,fftLength),1);
        timestamp = ii*tau_coh+readSkipTime;
        %function to calc SNR and Mean Noise Floor
        [sigpeak, meannoisef, snr] = snr_calc(fftXC,timestamp);
        SNR(ii)=snr;
        MNF(ii)=meannoisef;
    end
    jj=jj+1;
    Tau_coh(jj)=count;

    if jj == 1
        x = 0:1:40;
        x1=215:0.1:235;
    end
    SNR_max(jj)=max(SNR);
    %forming histograms of SNR and MNF
    [n,xout] = hist(SNR,x);
    snrhist(:,jj)=n./sum(n);
```

```
    [n1,xout1] = hist(MNF,x1);
    mnfhist(:,jj)=n1./sum(n1);
    clear n n1 SNR MNF

end
%%
%creating surface plots of SNR Vs no. of occurances Vs Tau_coh
figure;
surf(Tau_coh,x,snrhist)
shading interp
saveas(gcf,'SNR_surface_DVBT.fig')
%creating surface plots of MNF Vs no. of occurances Vs Tau_coh
figure;
surf(Tau_coh,x1,mnfhist)
shading interp
saveas(gcf,'MNF_surface_DVBT.fig')

clear all
toc


function [header,data] = readfile_NoSm_Skip_v2(varargin)
% [header,data] = readfile_NoSm_Skip_v2(filename,start_time,stop_time)
%
% Inputs:
%       filename    char        Filename containing data to be extracted
%       start_time  double      Time at which to start data extraction (s)
%       stop_time   double      Time at which to end data extraction (s)
% Outputs:
%       header      char        File header
%       data        double      Extracted data (samples x channel)

% disp('Function: readfile_NoSm_Skip_v2.m')

% check inputs
if nargin == 1
    % read full file
    filename = varargin{1};
    start_time = [];
    stop_time = [];
elseif nargin == 3
    % read partial file
    filename = varargin{1};
    start_time = varargin{2};
    stop_time = varargin{3};
else
    disp('Error!! Incorrect number of user inputs.')
    return
```

```
end

% memory map the header
m_hdr = memmapfile(filename,'Format',{'uint8' [1 1024] 'hdr'},'Repeat',1);
% read into matlab
header = char(m_hdr.data.hdr);
% display in command window
% header_decode(header)

% file details
file_det = dir(filename);
% number of samples in the file
num_samps_in_file = (file_det.bytes-1024)/16;
% disp(['Number of samples in file: ', num2str(num_samps_in_file)])
% length of file in seconds
file_time = num_samps_in_file/12.5e6;
% disp(['File recording time (s): ', num2str(file_time)])
% check stop_time and start_time
if isempty(start_time)
    % read full file
    start_time = 0;
    stop_time = file_time;
elseif start_time > stop_time
    disp('Error!! Start time must be less then stop time.')
    return
elseif stop_time > file_time
    disp('Warning, stop time greater then total file time...
     , truncating to total file time.')
    stop_time = file_time;
end
% convert time to samples
start_samp = floor(start_time*12.5e6);
stop_samp = floor(stop_time*12.5e6);
% start_samp = ceil(start_time*12.5e6/4)*4;
% stop_samp = ceil(stop_time*12.5e6/4)*4;
% number of required samples
num_samp = stop_samp - start_samp;
% compute required offset in bytes
file_offset = 1024 + start_samp*16;
% set the data region to be mapped in int16
file_region = [8 num_samp];
% memory map the data
m_data = memmapfile(filename,'Offset',file_offset,'Format',...
{'int16' file_region 'x'},'Repeat',1);

% try loading the mapped data into matlab
disp(sprintf('Loading mapped data into Matlab...'));
```

```
% tic
try
    % Complex Channel 1
    data(:,1) = complex(m_data.Data(1).x(2,:),m_data.Data(1).x(1,:));
    % Complex Channel 2
    data(:,2) = complex(m_data.Data(1).x(4,:),m_data.Data(1).x(3,:));
    % Complex Channel 3
    data(:,3) = complex(m_data.Data(1).x(6,:),m_data.Data(1).x(5,:));
    % Complex Channel 4
    data(:,4) = complex(m_data.Data(1).x(8,:),m_data.Data(1).x(7,:));
    % convert int16 to double precision (warning, quadruples data size!!)
    data = double(data);
catch
    % can't do it, not enough memory
    disp('Error!! Insufficient memory to load data');
    rethrow(lasterror)
    return
end
% toc
disp(sprintf('Done!\n'));


function [peak,meannoise_floor, SNR] = snr_calc(fftXC,timestamp)

peak= max(max(20*log10(abs(fftXC(1:62,:)))));
peak1 = max(max(20*log10(abs(fftXC(69:end,:)))));
peak = max([peak peak1]);
a=mean(mean(20*log10(abs(fftXC(1:62,:)))));
a1=mean(mean(20*log10(abs(fftXC(69:end,:)))));
meannoise_floor=mean([a a1]);
SNR = peak - meannoise_floor;
```

DEFENCE SCIENCE AND TECHNOLOGY ORGANISATION DOCUMENT CONTROL DATA	1. CAVEAT/PRIVACY MARKING

2. TITLE	3. SECURITY CLASSIFICATION
A new Illuminator of Opportunity Bistatic Radar Research Project at DSTO	Document (U) Title (U) Abstract (U)
4. AUTHORS	5. CORPORATE AUTHOR
James Palmer, Simon Palumbo, Tri-Tan Van Cao and Stephen Howard	Defence Science and Technology Organisation PO Box 1500 Edinburgh, South Australia 5111, Australia

6a. DSTO NUMBER	6b. AR NUMBER	6c. TYPE OF REPORT	7. DOCUMENT DATE
DSTO–TR–2269	AR–014–429	Technical Report	May, 2009

8. FILE NUMBER	9. TASK NUMBER	10. SPONSOR	11. No OF PAGES	12. No OF REFS
2008/1116464	LRR 07/247		81	36

13. URL OF ELECTRONIC VERSION	14. RELEASE AUTHORITY
http://www.dsto.defence.gov.au/corporate/reports/DSTO–TR–2269.pdf	Chief, Electronic Warfare and Radar Division

15. SECONDARY RELEASE STATEMENT OF THIS DOCUMENT

Approved For Public Release

OVERSEAS ENQUIRIES OUTSIDE STATED LIMITATIONS SHOULD BE REFERRED THROUGH DOCUMENT EXCHANGE, PO BOX 1500, EDINBURGH, SOUTH AUSTRALIA 5111

16. DELIBERATE ANNOUNCEMENT

No Limitations

17. CITATION IN OTHER DOCUMENTS

No Limitations

18. DSTO RESEARCH LIBRARY THESAURUS

Waveform Analysis
Target Tracking
Target Detection
Research Projects

19. ABSTRACT

In this report a new Illuminator of Opportunity / Passive Coherent Location research project being conducted in the Microwave Radar Branch of EWRD at DSTO is discussed. Details are provided about such aspects as transmitter selection and characteristics, experimental configurations and power budget studies. Furthermore, a preliminary analysis of two different transmitters' waveform ambiguity functions is presented. Early results from field experiments demonstrating detections of cars, trucks, trains, helicopters and aircraft using a terrestrial digital TV and geosynchronous satellite signals are also presented. The ability to detect and track targets is then demonstrated through the use of several CFAR and Track Before Detect algorithms. The report concludes by discussing potential application areas for this technology as well as highlighting the likely directions of future research.